THE ROLE OF STAT3 IN SKELETAL DEVELOPMENT

by

Rebecca Davidson

A Thesis

Submitted to the Faculty of Purdue University

In Partial Fulfillment of the Requirements for the degree of

Master of Science

Department of Biological Sciences

Indianapolis, Indiana

August 2017

THE PURDUE UNIVERSITY GRADUATE SCHOOL
STATEMENT OF COMMITTEE APPROVAL

Dr. Jiliang Li, Chair

Department of Biology

Dr. Hiroki Yokota

Department of Biomedical Engineering

Dr. Kathleen Marrs

Department of Biology

Approved by:

Dr. Theodore Cummins

Head of the Graduate Program

To my friends and family,

You are the motivation behind everything I do.

ACKNOWLEDGMENTS

I would first and foremost like to thank my mentor, Dr. Jiliang Li, without whom none of this would have been possible. The lessons he taught me and advice he gave will stay with me as I move on to future stages of my scientific career. I would also like to thank Dr. Hiroki Yokota for serving on my committee as well as opening his lab to me to perform countless experiments that contributed to my projects. I would like to thank Dr. Kathleen Marrs for also serving on my committee and helping me be a better teacher and mentor. In the Yokota lab, I would like to thank Shinya Takigawa, Nhi TruongVo, Shengzhi Liu, and Luqi Wang for providing their expertise and assistance as I learned my way around their lab, as well as Andy Chen for his work on the microarray analysis. For his help in histology, I would like to thank Yongqi Yu. For their assistance in countless experiments that went toward my projects, I would like to thank Li lab members Andrew Nguyen, Yukun Yin, Aihua Xu, Michalein Dickinson, Erika Gramelspacher, Kaity Jones, Chelsea Smith, Hannah Beers, Anu Yedanaparthi, Megan Wheeler, and Alison Prose. Their willingness to help as well as their friendship mean so much to me, and they helped make my time as a graduate student a fun and memorable experience.

TABLE OF CONTENTS

LIST OF TABLES viii
LIST OF FIGURES ix
ABSTRACT xiii
CHAPTER 1. INTRODUCTION 1
1.1 Bone Biology 1
1.2 Skeletal Macrostructure 1
1.3 Skeletal Microstructure 2
1.4 Bone Composition 3
1.5 Bone Cells 3
1.5.1 Osteoclasts 3
1.5.2 Osteoblasts 5
1.5.3 Other Bone Cells 6
1.6 Signaling Among Bone Cells 7
1.7 Skeletal Development 7
1.7.1 Endochondral Bone Development 7
1.7.2 Intramembranous Bone Development 8
1.8 Bone Modeling and Remodeling 8
1.8.1 Bone Modeling 8
1.8.2 Bone Remodeling 9
1.9 STAT Overview 9
1.10 STAT Activation 10
1.11 STAT Transcription 11
1.12 STAT Regulation 11
1.13 Stat3 12
1.14 Stat3 in Hyper-IgE Syndrome (HIES) 13
1.14.1 HIES Characterization 13
1.14.2 HIES Mutations 13
1.15 Stat3 Effect on Bone 14
1.16 Research Goals 16

CHAPTER 2. MATERIALS AND METHODS 18
2.1 *In vivo* Mouse Study 18
2.1.1 Experimental Mice 18
2.1.2 Breeding Scheme 18
2.1.3 Genotyping 18
2.1.4 Sacrificing 19
2.1.5 Bone Mineral Density and Content 20
2.1.6 Micro-Computed Tomography (CT) 20
2.1.7 Histology 20
2.1.7.1 Slide Preparation of Midshaft 20
2.1.7.2 Slide Preparation of Distal 21
2.1.8 Dynamic Histomorphometry 21
2.2 Osteoclast Preparation 22
2.2.1 Cell Culture 22
2.2.1.1 Stat3 Suppression 22
2.2.1.2 Stat3 Overexpression 22
2.2.2 Protein Collection 23
2.2.3 Calculating Protein Concentration 24
2.2.4 RNA Collection 24
2.2.5 RT-PCR 25
2.2.6 qPCR 25
2.2.7 Western Blot 25
2.2.8 Microarray 27
2.2.9 TRAP Staining 27
2.3 Statistical Analysis 28
CHAPTER 3. RESULTS 29
3.1 OSX-Cre Stat3-LoxP cKO 8-Week Mouse Models 29
3.1.1 Phenotypes 29
3.1.2 Micro-CT Analysis 30
3.1.3 Dynamic Histomorphometry Measurements 31
3.2 Osteoclast Stat3 siRNA and Overexpression 31

3.2.1 Microarray Analysis 31
3.2.2 mRNA Expression Patterns 32
3.2.3 Protein Production Patterns 32
3.2.3.1 Stat3 siRNA Knockdown 32
3.2.3.2 Stat3 Overexpression Construct 33
3.2.4 TRAP Staining 33
CHAPTER 4. DISCUSSION 34
4.1 Osterix Cre Stat3 KO in Osteoblasts 34
4.2 Osteoclast *in vitro* Analysis 36
4.3 Future Directions 38
REFERENCES 41
TABLES 45
FIGURES 47

LIST OF TABLES

Table 1: Comprehensive qPCR primer list 45
Table 2: KEGG pathway analysis based on microarray data 46

LIST OF FIGURES

Figure 1: Intracellular pathway of osteoclast being induced by RANKL (Okamoto and Takayanagi)..... 47
Figure 2: Osteoblast differentiation pathway (Arboleya and Castañeda)..... 48
Figure 3: Stat3 signaling pathways (Yu et al.)..... 49
Figure 4: Stat3 structure with listed mutations (Holland et al.)..... 50
Figure 5: Stat3-C Flag pRc/CMV 7969 bp overexpression construct (Bromberg et al.). 51
Figure 6: Body weights of experimental mice at 8 weeks of age. Highly significant decrease in weight observed between WT males and cKO males as well as WT females and cKO females. 52
Figure 7: Female WT (left) and female cKO (right) at 7 weeks..... 53
Figure 8: Dissected femurs of male (left) and female (right) 8-week mice. In both images, the femur to the left is WT and the femur to the right is cKO. Both sexes exhibited a highly significant decrease in length in cKO in comparison to their WT counterparts. 54
Figure 9: Femur lengths of experimental mice at 8 weeks of age. Highly significant decrease in femur length observed between WT males and cKO males as well as WT females and cKO females..... 55
Figure 10: Bone mineral density of experimental mice at 8 weeks of age. No significant difference between WT males and cKO males. Significant decrease in BMD observed between WT females and cKO females. 56
Figure 11: Bone mineral content of experimental mice at 8 weeks of age. Significant decrease observed between WT males and cKO males as well as WT females and cKO females..... 57
Figure 12: Micro CT analysis of 8-week mouse femurs. From left to right: WT males (A), cKO males (B), WT females (C), and cKO females (D). cKO mice of both sexes had shorter femurs that had a metaphyseal defect indicated by the arrow.. 58

Figure 13: Total volume of cortical region based on Micro-CT analysis in experimental mice at 8 weeks of age. Highly significant decrease observed between male WT and cKO mice. Significant decrease observed between female WT and cKO mice. 59
Figure 14: Bone volume of cortical region based on Micro-CT analysis in experimental mice at 8 weeks of age. Highly significant decrease observed between male WT and cKO mice. Significant decrease observed between female WT and cKO mice. 60
Figure 15: Bone volume over tissue volume of cortical region based on Micro-CT analysis in experimental mice at 8 weeks of age. No significant changes were seen between WT or cKO in either the males or the females. 61
Figure 16: Total surface area and perimeter of cortical region based on Micro-CT analysis in experimental mice at 8 weeks of age. No significant changes were seen between WT or cKO in either the males or the females. 62
Figure 17: Bone surface area and perimeter of cortical region based on Micro-CT analysis in experimental mice at 8 weeks of age. A significant decrease was seen from the WT to the cKO males in both categories. No significant change was seen in females. 63
Figure 18: Bone surface over bone volume of cortical region based on Micro-CT analysis in experimental mice at 8 weeks of age. A highly significant increase was seen from the WT to the cKO in both males and females. 64
Figure 19: Dynamic histomorphometry of trabecular region showing mineralizing surface over bone surface. A significant increase was seen in cKO females compared to WT females. No significant difference was seen in males. 65
Figure 20: Endocortical surface parameters showing significant decrease in cKO females for mineralizing surface over bone surface, mineral apposition rate, and bone formation rate over bone surface. No significant difference was seen in males. 66

Figure 21: Periosteal surface parameters showing significant increase in cKO females for mineral apposition rate and bone formation rate over bone surface. No significant difference was seen for either sexes in mineralizing surface over bone surface. No significant change was seen in males. 67
Figure 22: Microarray heat map of 24 hour RANKL samples. 68
Figure 23: qPCR analysis of Stat3 primer showing highly significant knockdown compared to non-specific controls. 69
Figure 24: qPCR analysis of genes upregulated in Stat3 siRNA 24 hour RANKL groups. 70
Figure 25: qPCR analysis of genes downregulated in Stat3 siRNA 24 hour RANKL groups. 71
Figure 26: Western blot b-actin bands of Stat3 siRNA knockdown samples quantified with relative density at 6 hours (A) and 24 hours (B). Each band from left to right represents pre-osteoclast control, pre-osteoclast with Stat3 siRNA, RANKL-stimulated osteoclast control, and RANKL-stimulated with Stat3 siRNA. 72
Figure 27: Western blot p-Stat3 bands of Stat3 siRNA knockdown samples quantified with adjusted density to b-actin at 6 hours (A) and 24 hours (B). Each band from left to right represents pre-osteoclast control, pre-osteoclast with Stat3 siRNA, RANKL-stimulated osteoclast control, and RANKL-stimulated with Stat3 siRNA. 73
Figure 28: Western blot NFATc1 bands of Stat3 siRNA knockdown samples quantified with adjusted density to b-actin at 6 hours (A) and 24 hours (B). Each band from left to right represents pre-osteoclast control, pre-osteoclast with Stat3 siRNA, RANKL-stimulated osteoclast control, and RANKL-stimulated with Stat3 siRNA. 74
Figure 29: Western blot c-Fos bands of Stat3 siRNA knockdown samples quantified with adjusted density to b-actin at 6 hours (A) and 24 hours (B). Each band from left to right represents pre-osteoclast control, pre-osteoclast with Stat3 siRNA, RANKL-stimulated osteoclast control, and RANKL-stimulated with Stat3 siRNA. 75

Figure 30: Western blot Cathepsin K bands of Stat3 siRNA knockdown samples quantified with adjusted density to b-actin at 24 hours (A). Each band from left to right represents pre-osteoclast control, pre-osteoclast with Stat3 siRNA, RANKL-stimulated osteoclast control, and RANKL-stimulated with Stat3 siRNA. 76
Figure 31: Western blot b-actin bands of Stat3 overexpression construct samples quantified with relative density at 6 hours (A). Each band from left to right represents pre-osteoclast control, pre-osteoclast with Stat3 construct, RANKL-stimulated osteoclast control, and RANKL-stimulated with Stat3 construct. 77
Figure 32: Western blot p-Stat3 bands of Stat3 overexpression construct samples quantified with relative density at 6 hours (A). This graph illustrates the significant increase in Stat3 production for both overexpression groups. 78
Figure 33: Western blot NFATc1 bands of Stat3 overexpression construct samples quantified with relative density at 6 hours (A). This graph illustrates there is no significant difference between the RANKL groups when Stat3 is overexpressed. 79
Figure 34: Western blot c-Fos bands of Stat3 overexpression construct samples quantified with relative density at 6 hours (A). This graph demonstrates a slight but insignificant increase in c-Fos production when Stat3 is overexpressed..... 80
Figure 35: TRAP-stained RAW 264.7 cells stimulated with RANKL. A significant increase in multi-nucleated osteoclasts was observed when Stat3 was knocked down. 81
Figure 36: TRAP-stained RAW 264.7 cells. From left to right, top to bottom: non-specific siRNA without RANKL (A), Stat3 siRNA without RANKL (B), non-specific siRNA with RANKL (C,E), and Stat3 siRNA with RANKL (D,F). 82

ABSTRACT

Author: Davidson, Rebecca. MS
Institution: Purdue University
Degree Received: August 2017
Title: The Role of Stat3 in Skeletal Development.
Major Professor: Jiliang Li

Many factors are present in the development of skeletal tissue. Some factors lead to an increase in bone mass while some lead to a decrease. One factor that is known to have an influence on skeletal development is Signal Transducer and Activator of Transcription 3 (Stat3). This knowledge arose because of a mutation in the Stat3 gene in humans causing a disease called Hyper-IgE Syndrome. This mutation leads to a variety of issues, including decreased bone mass. Because of this, our lab has sought to study Stat3 in its relation to bone. Many studies have already been conducted that discern how Stat3 influences skeletal biology by observing its role in osteoclasts, osteoblasts, and other bone cells. Its role is still unclear, and many studies have provided seemingly contradictory results in how it works on bone tissue. Our lab set up several different studies in order to further elucidate what role Stat3 plays in skeletal development by looking at its effects on osteoblasts and osteoclasts, the bone-forming and bone-destroying cells of the body, respectively.

We conditionally knocked out Stat3 in the osteoblasts of mice and compared several different bone parameters to their wild type counterparts at 8 weeks of age. Differences were noted in bone phenotype, including decreased femur length, weight, bone mineral density, and bone mineral content in the cKO compared to their WT counterparts. While no significant difference in trabecular integrity was noted, several differences were observed in cortical bone. These differences indicate that Stat3 has a positive role in osteoblast differentiation, leading to an overall positive effect on bone mass.

To observe the role of Stat3 in osteoclasts, *in vitro* experiments were set up in which pre-osteoclast RAW 264.7 cells were manipulated with Stat3 siRNA or a Stat3 overexpression construct and RANKL to induce differentiation. Using qPCR and western

blot assays, it was determined that when Stat3 is knocked down, several important genes in osteoclastogenesis and osteoclast function are more highly expressed than in the control groups. When Stat3 is overexpressed, a similar pattern is observed where these same genes are downregulated in the presence of higher Stat3 levels. These results indicate that Stat3 has an overall inhibitory effect on osteoclastogenesis and osteoclast function, indicating it has a positive effect on bone mass.

Future studies could be performed to further elucidate the effects of Stat3 on skeletal development. Isolating the osteoblasts from cKO and WT mice and performing qPCR and western blot assays could be useful in finding out how Stat3 is influencing these cells. Further studies could also be done on the RAW 264.7 cells to find where Stat3 is interacting with the RANKL pathway. A resorption assay could be done with these cells to better understand how function might be influenced by Stat3.

CHAPTER 1. INTRODUCTION

1.1 Bone Biology

Bones serve many different purposes inside the body. They act as an anchor for muscles to support movement as well as a shield for the most delicate of internal organs (Clarke). Bones provide mechanical strength and are necessary for load bearing (Burr and Ozan). They aid the body in mineral homeostasis by providing storage for ions such as calcium that can be released when needed for different cellular pathways and muscle contraction (Burr and Ozan). They are also the site of hematopoiesis and play an important role in endocrine function (Burr and Ozan). Bone is clearly an exceptionally important organ, however unobvious this fact may be at first glance. Knowing what bones consist of and how they are created on a cellular and molecular level can aid in the discovery of new medications and therapies that seek to treat bone diseases such as osteoporosis and osteopenia.

1.2 Skeletal Macrostructure

The vertebrate skeleton is divided into two parts: the axial skeleton and the appendicular skeleton (Solomon, Berg and Martin). Within the appendicular skeleton are the bones of the upper and lower extremities, many of which are long bones (Solomon, Berg and Martin). These bones are made up of a long shaft called the diaphysis, and two ends referred to as the epiphyses (Solomon, Berg and Martin). The metaphysis is an area of growth between the diaphysis and epiphysis that exists in youth, but disappears in later development (Solomon, Berg and Martin). A sheath of connective tissue called the periosteum surrounds the long bone, and the endosteum surrounds a hollow cavity within the bone which houses the bone marrow (Solomon, Berg and Martin). The diaphysis in the long and short bones of the skeleton is made up primarily of cortical bone, which is relatively dense and compact (Burr and Ozan). This type of bone contains Haversian canals that offer some porosity to its otherwise solid structure (Burr and Ozan). However, cortical bone is still sturdy and strong, which allows for structural support and protection (Burr and Ozan). The metaphyses in the long bones of the skeleton are made up primarily

of cancellous bone, which is much more porous than cortical bone (Burr and Ozan). Sometimes referred to as spongy or trabecular bone, cancellous bone is mainly composed of long rods, or trabeculae, connected to each other in a meshwork that allow for mechanical strength (Burr and Ozan). Within this meshwork is a hollow space for bone marrow to reside (Burr and Ozan).

1.3 Skeletal Microstructure

A large portion of the bone is made up of lamellae, which are concentric circles comprised of mineral and collagen (Burr and Ozan). These lamellae can be found around the periosteum and endosteum and within trabeculae (Burr and Ozan). Unlike lamellar bone, woven bone is not well organized due to rapid formation rate (Burr and Ozan). Woven bone is laid down quickly, typically due to an urgent need for new bone as in times of damage or great mechanical stress (Burr and Ozan). During woven bone formation, collagen fibers are rapidly deposited and mineralized (Burr and Ozan). Unlike woven bone which can be deposited without any pre-existing surface, primary bone must be deposited onto cartilage or bone that has already been formed (Burr and Ozan). There are three different types of primary bone: primary lamellar bone, plexiform bone, and primary osteons (Burr and Ozan). All of these types of primary bone differ in how they are organized and what their function is (Burr and Ozan). Primary lamellar bone is deposited in dense lamellar sheets, which provide strength to periosteal, endosteal, and trabecular surfaces (Burr and Ozan). Plexiform bone is used for rapid growth (Burr and Ozan). The non-lamellar portion is deposited de novo and primary lamellar bone is deposited on the surface (Burr and Ozan). Lastly, primary osteons form on the surface of large vascular canals, essentially decreasing the diameter of these canals by adding several osteonal layers on the inside (Burr and Ozan). Secondary bone is another bone type that differs from primary bone in that it uses highly coordinated coupling of resorption and formation on a pre-existing bone surface (Burr and Ozan). Interstitial bone is the type of bone that is left untouched during the remodeling process (Burr and Ozan).

1.4 Bone Composition

The three main components of bone are water, organic material, and mineral (Burr and Ozan). The main mineral found in bone is carbonated apatite, and the organic material consists mostly of type I collagen, as well as NCPs (noncollagenous proteins) that are mainly extracellular but also exist within the bone cell (Burr and Ozan). Among these noncollagenous proteins are proteoglycans, glycosaminoglycans, glycoproteins, and other proteins such as osteocalcin and osteonectin (Burr and Ozan). These noncollagenous proteins are important in roles such as controlling mineral deposition (Burr and Ozan).

Collagen plays an important role in the bone of retaining flexibility and suppleness, while the main role of mineral is to provide rigidity (Burr and Ozan). Water is also an important component of the bone because without it, the bone will become too stiff and can break more easily (Burr and Ozan). The way in that the collagen and mineral are deposited dictates what type of function they might have and what the newly forming bone can be used for (Burr and Ozan). If the bone forms rapidly in a more unorganized fashion, this could mean the bone was needed for a quick repair (Burr and Ozan). However, if the bone deposits more slowly and carefully, this could mean the bone was needed in response to mechanical loading that created microfractures (Burr and Ozan).

1.5 Bone Cells

1.5.1 Osteoclasts

Within the bone, there are several different cell types. One of these types of cells is osteoclasts, which are responsible for breaking bone down (Bellido, Plotkin and Bruzzaniti). Osteoclasts are derived from the hematopoietic cell progenitor line that also gives rise to macrophages and monocytes (Z. Zhang et al.). Which type of cell the progenitor becomes is dependent on which factors are present in the environment, essentially dictating what type of stimulation they will receive to differentiate. Osteoclasts are stimulated by Receptor Activator of Nuclear factor Kappa-B Ligand (RANKL), a member of the Tumor Necrosis Factor (TNF) ligand family, which activates a pathway leading to the release of several different factors that cause bone to break down (Bellido, Plotkin and Bruzzaniti). Upon RANKL binding to Receptor Activator of

Nuclear factor Kappa-B (RANK) on the osteoclast surface, TNF receptor-associated factor 6 (TRAF6) is activated, causing a cascade that ultimately induces osteoclast differentiation, also referred to as osteoclastogenesis (Bellido, Plotkin and Bruzzaniti). Nuclear factor-kappa B (Nfkb) is a highly important factor in this cascade, causing the upregulation of c-Fos which, in turn, upregulates nuclear factor of activated T-cells 1 (NFATc1) (Bellido, Plotkin and Bruzzaniti). (Figure 1) NFATc1 is critical for differentiation of osteoclasts and remains an intensely studied transcription factor in osteoclastogenesis.

When bone needs to be broken down, osteoclast precursors arrive at the bone surface, proliferate, differentiate, and fuse into multi-nucleated osteoclasts (Bellido, Plotkin and Bruzzaniti). Osteoclast precursors are recruited to the site by several factors which include calcium gradients and osteoblast-mediated signaling (Bellido, Plotkin and Bruzzaniti). Once they arrive at the bone surface, several growth factors come into play to cause them to proliferate into committed mono-nucleated pre-osteoclasts (Bellido, Plotkin and Bruzzaniti). They then differentiate in response to RANKL expressed on the surface of osteoblasts and osteocytes (Bellido, Plotkin and Bruzzaniti). RANKL and several other factors, including V-ATPase subunit D2, also assist in osteoclast fusion to form multinucleated cells (Bellido, Plotkin and Bruzzaniti).

Once the osteoclast has fused, it attaches itself to the bone surface where polarization of the cell occurs (Bellido, Plotkin and Bruzzaniti). The area of the cell on the bone surface is the apical side, where the factors needed to break the bone down are secreted (Bellido, Plotkin and Bruzzaniti). Direct contact of the cell to the bone surface is made through an area known as the sealing zone where podosomes consisting of filamentous actin on the apical surface of the osteoclast touch the bone surface (Bellido, Plotkin and Bruzzaniti). Inward of the sealing zone is a transition zone to the ruffled border (Bellido, Plotkin and Bruzzaniti). There is a gap of space in between the ruffled border and bone surface where factors are secreted that result in bone dissolution (Bellido, Plotkin and Bruzzaniti).

In order to begin tearing up the unwanted areas of bone, the osteoclast releases several factors onto the bone surface. Carbonic anhydrases create protons which vacuolar

ATPases then release into the environment between the osteoclast and the bone surface, causing it to become acidic (Bellido, Plotkin and Bruzzaniti). Cathepsin K is also released, which is a protease that eats away at the collagenous bone matrix (Bellido, Plotkin and Bruzzaniti). The degraded material is engulfed inside the osteoclast by vacuoles that move to lysosomes, bringing the broken-down bone material into the cell to be further processed and used for other cellular processes (Bellido, Plotkin and Bruzzaniti).

At the conclusion of the bone resorption event, osteoclast apoptosis occurs (Bellido, Plotkin and Bruzzaniti). This process is currently not well understood. However, there are several factors that likely lead to osteoclast cell death. Calcium that is released by the degraded bone material potentially helps trigger this event, as well as Fas ligand secreted by osteoblasts and integrin signaling (Bellido, Plotkin and Bruzzaniti). The down-regulation of anti-apoptotic factors such as RANKL and M-CSF could also contribute to this programmed cell-death (Bellido, Plotkin and Bruzzaniti).

1.5.2 Osteoblasts

Another type of bone cell is osteoblasts, which are needed to form new bone (Bellido, Plotkin and Bruzzaniti). These cells are derived from the mesenchymal stem cell lineage that also gives rise to chondrocytes and adipocytes (Fakhry et al.). Mesenchymal stem cells receive signals from proteins such as Wnts, bone morphogenic protein (BMP)-2, and parathyroid hormone (PTH) to induce differentiation into the osteoblast lineage (Kapinas et al.). (Figure 2) Wnts play a role in several different time points throughout the differentiation process (Kapinas et al.). They help MSCs proliferate, aid in committing the cells to being osteo-chondro precursors, and work to prevent osteoblast apoptosis (Bellido, Plotkin and Bruzzaniti; Kapinas et al.). The osteo-chondro precursers are then induced by factors such as Runx2 in order to become preosteoblasts (Bellido, Plotkin and Bruzzaniti). Further induction occurs into immature osteoblasts, followed by their final form as mature osteoblast cells (Bellido, Plotkin and Bruzzaniti). Once these mature osteoblasts have finished forming new bone matrix, they either undergo apoptosis, differentiate further into osteocytes that embed into the newly formed bone, or remain on the inactive bone surface as lining cells (Bellido, Plotkin and Bruzzaniti).

Osteoblast progenitors proliferate and are maintained by several transcription factors prior to differentiation (Bellido, Plotkin and Bruzzaniti). Runx2 and Osterix are two crucial transcription factors in osteoblastogenesis that are controlled by a variety of extracellular ligands such as the WNTs, BMPs, and FGFs, and are needed in order to activate several genes involved in bone formation (Bellido, Plotkin and Bruzzaniti; Y. Zhang et al.). After osteoblasts proliferate, they begin depositing bone matrix proteins such as type I collagen and mineralizing this bone to form osteoid (Bellido, Plotkin and Bruzzaniti). This is most often followed by cell death (Bellido, Plotkin and Bruzzaniti). Each of these stages is distinct in that different genes are turned on and different markers are expressed (Bellido, Plotkin and Bruzzaniti).

1.5.3 Other Bone Cells

Aside from osteoblasts and osteoclasts, there are several other bone cells that play critical roles in maintaining bone homeostasis. One such cell is the osteocyte, discussed previously. This cell type forms from osteoblasts that have become encased within newly formed bone (Bellido, Plotkin and Bruzzaniti). This encasement is likely a deliberate process that keeps the osteocytes in an ideal position within lacuna in the newly formed matrix (Dallas, Prideaux and Bonewald). They are important for mediating signals between other bone cells and sensing when stress has been put on different areas of the bone. While these mechanisms are still not well-understood, it has been proposed that osteocytes sense this strain through the cell body, glycocalyces on dentritic processes, and/or cilia bending (Bonewald). The dendrites move through canaliculi in order to make contact with bone cells and the vasculature woven through the matrix (Dallas, Prideaux and Bonewald). They are able to contact and communicate with other cells that have connexin43 (Cx43) gap junctions (Buo and Stains).

Monocytes and macrophages have also been shown to have an important role in osteoblast differentiation by producing oncostatin M (OSM) which leads to a signaling cascade that causes osteoblasts to differentiate from mesenchymal stem cells (MSCs) (Nicolaidou et al.).

1.6 Signaling Among Bone Cells

When mechanical strain is placed on the bone, or there is not enough strain on the bone to justify its current mass, different signals must be sent out in order to recruit the proper cells to the site that can fix the issue. Bone marrow stromal cells (BMSCs), osteoblasts, and osteocytes all express M-CSF and RANKL, which are essential for osteoclast differentiation (Bellido, Plotkin and Bruzzaniti). Additionally, osteoblasts and osteocytes secrete osteoprotegerin (OPG) which can bind RANKL, preventing its induction of the cellular pathway that leads to osteoclastogenesis (Bellido, Plotkin and Bruzzaniti). OPG essentially negatively regulates osteoclastogenesis and an imbalance of OPG in relation to RANKL can cause issues that lead to osteoporotic or osteopetrotic phenotypes (Teitelbaum).

1.7 Skeletal Development

1.7.1 Endochondral Bone Development

There are two main types of bone development: endochondral and intramembranous (Solomon, Berg and Martin). Endochondral bone development occurs mainly in the long bones (Solomon, Berg and Martin). This kind of bone development creates a cartilaginous template that can later be ossified (Solomon, Berg and Martin) Endochondral ossification begins with a cluster of mesenchymal stem cells differentiating into chondroblasts with the help of transcription factor SOX-9 (Allen and Burr) These chondroblasts produce a cartilaginous matrix that resembles the final bone shape (Allen and Burr) Chondroblasts that embed within the cartilage become chondrocytes, and the cartilage itself becomes surrounded by a perichondrium (Allen and Burr) This perichondrium contains cells that differentiate into osteoblasts via transcription factor RUNX2, and deposit bone matrix onto the cartilage template (Allen and Burr) This newly forming lamellar bone takes over around the diaphysis, turning the perichondrium into periosteum (Allen and Burr). As the area becomes vascularized, a primary ossification center appears that will continue to aid the development of the bone (Allen and Burr). A secondary ossification center also appears in the epiphysis (Allen and Burr). The junction between the diaphysis and epiphysis, referred to as the epiphyseal or growth plate,

contains different regions of cells that aid in longitudinal growth (Allen and Burr). There are five different zones of cells in this area from the furthest to the primary ossification center to the nearest: the resting zone, the proliferative zone, the hypertrophic zone, the calcified cartilage zone, and the zone of ossification (Allen and Burr). During this process, osteoclast precursors are recruited to the mesenchyme surrounding the bone where they proliferate and differentiate before moving through the bone collar and hollowing out the marrow cavity within the developing long bone (Engsig et al.).

1.7.2 Intramembranous Bone Development

Intramembranous ossification occurs in the bones of the skull as well as the clavicles (Allen and Burr). This type of bone formation occurs mainly through the use of mesenchymal stem cells that, through expression of RUNX2, are driven directly into differentiating into osteoblasts (Allen and Burr). These osteoblasts then rapidly form woven bone that they later can add more woven bone or primary lamellar bone onto (Allen and Burr).

1.8 Bone Modeling and Remodeling

1.8.1 Bone Modeling

Bone modeling occurs during skeletal development when bone is being either formed by osteoblasts or resorbed by osteoclasts on a pre-existing surface (Solomon, Berg and Martin). Formation modeling occurs when osteoblasts are recruited to the site, while resorptive modeling occurs when osteoclasts are recruited to the site (Allen and Burr). Modeling will occur when either cell is activated and used to either resorb or form bone (Allen and Burr). Either type of modeling can occur on either trabecular, endosteal, or periosteal surfaces (Allen and Burr). Formation modeling will occur when a certain level of strain has occurred in a certain area of the bone, while resorptive modeling will occur when too low an amount of strain has been placed on the bone (Allen and Burr). This ensures that there is always an appropriate amount of bone relative to the strain being placed on the bone. Forming new bone is expensive, so only performing formation modeling when there is too much strain is essential. Bone also contains precious materials such as calcium that the body could use for other important processes if the

bone does not need as much strength in that area. Modeling involves both an activation stage and a formation or resorption phase (Allen and Burr). Depending on the level of strain occurring in the surrounding tissue, the activation stage will involve the recruitment of precursors that will either differentiate into osteoblasts or osteoclasts, and the bone will either be formed or resorbed respectively (Allen and Burr). Lining cells already on the bone surface can also be called upon to differentiate back into mature osteoblasts and deposit new bone matrix (Allen and Burr). In bone modeling, formation and resorption occur on different surfaces of the bone, often in order to support radial growth or shift the cortex from the central axis (Allen and Burr). Essentially, bone will be resorbed on the endosteal surface and formed on the periosteal surface (Allen and Burr).

1.8.2 Bone Remodeling

Remodeling occurs during the adult lifespan when old bone needs to be removed and replaced with new bone (Solomon, Berg and Martin). Both osteoblasts and osteoclasts play a role in this process (Solomon, Berg and Martin). Unlike in bone modeling, resorption and formation occur sequentially when the bone is being remodeled (Solomon, Berg and Martin). In remodeling, the mechanism is activation followed by resorption followed by formation (Allen and Burr). Essentially, osteoclasts begin the process by initiating the resorption event, a transition occurs moving from resorption to formation, and osteoblasts finish the process by forming the new bone (Florencio-Silva et al.). The coordination between osteoclasts and osteoblasts in this process must be finely tuned to maintain the proper structure of the bone surface being remodeled (Andersen et al.). Once osteoclasts have finished resorbing the damaged bone, they recruit osteoblasts both indirectly via the release of growth factors from the broken-down bone matrix as well as directly through making contact with these osteoblasts and releasing certain secreted factors (Khosla, Oursler and Monroe).

1.9 STAT Overview

Signal Transduction and Activation of Transcription (STAT) family transcription factors are activated by Janus Kinase 2 (JAK2) and mediate cell survival, differentiation, and proliferation (Lodish et al.; Zhou et al.). There are seven different STAT proteins in

mammals: STAT1, STAT2, STAT3, STAT4, STAT5A, STAT5B, and STAT6 (Timofeeva et al.). Each of these proteins consists of an N-terminal domain with oligomerization and coiled-coil domains, a DNA binding domain (DBD), a linker domain, a Src homology 2 (SH2) domain, and a C-terminal transactivation domain on which phosphorylation can occur (Lodish et al.; Timofeeva et al.; Fagard et al.).

Different cytokines and growth factors can activate different receptors on the cell surface that induce different signals through the cell (Lodish et al.). These receptors are attached to a JAK2 kinase on the cytosolic side of the membrane that can phosphorylate STAT transcription factors within the cell (Lodish et al.).

1.10 STAT Activation

Activation of STAT begins with a cytokine or growth factor binding to a receptor (Lodish et al.). These receptors for STAT activation have an extracellular domain where the cytokine or growth factor can bind, and an intracellular domain associated with JAK kinases (Lodish et al.). JAK proteins can associate with GPCRs, LIF-Rs, IL-Rs, and gp130 (Carpenter and Lo). Upon ligand binding, a conformation change occurs in the receptor, causing the JAK kinase domains to come together and phosphorylate each other on a specific tyrosine on the activation lip (Lodish et al.). The activation lips move away from the active site and the JAK proteins phosphorylate several tyrosines on the cytosolic end of the cytokine receptor (Lodish et al.). These phosphotyrosines act as docking sites for SH2 domains to bind (Lodish et al.). Since STAT proteins contain an SH2 domain, they are able to bind the docking site and become phosphorylated by JAK on the C-terminal domain on Y705/S727 (Lodish et al.; Xu et al.). Phosphorylation of STAT causes its dissociation from the receptor and dimerization with another STAT protein (Lodish et al.). The SH2 domain of either STAT associates with the phosphotyrosine on the other STAT (Lodish et al.). The proteins can either form a homodimer with the same kind of STAT protein or a heterodimer with a different kind of STAT protein (Delgoffe and Vignali). The Nuclear Localization Sequence (NLS) sites within the coiled-coil and dimer-dependent DNA-binding domains on the STAT dimer are exposed in this

conformation, allowing the dimer to easily move into the nucleus and bind the enhancer on a DNA molecule (Lodish et al.; Fagard et al.).

1.11 STAT Transcription

The DBD of the STAT homodimer either binds interferon gamma-activated sequence (GAS) or serum-induced element (SIE) which both reside in the promoter region of the desired target gene (Timofeeva et al.; Xu et al.). One SIE that STAT can bind lies in the promoter region of cellular (c)-Fos (Cressman, Diamond and Taub). Other promoters that specific STAT proteins can bind include p53, MMP-9, and IL-6 (Carpenter and Lo).

1.12 STAT Regulation

There are several methods the cell can use to regulate the JAK/STAT pathway. One method, used for short-term regulation, is through the activation of SHP1 (Lodish et al.). This phosphotyrosine phosphatase has an SH2 domain that binds a phosphotyrosine on a cytokine receptor, revealing another active site on the protein (Lodish et al.). This active site can essentially pull off the phosphate group on the JAK kinase, causing its inactivation (Lodish et al.).

Another method, used for long-term regulation, is through the recruitment of the SOCS protein (Lodish et al.). SOCS is activated by the JAK/STAT signaling pathway, creating a negative feedback loop (Lodish et al.). SOCS has an SH2 domain that can bind phosphotyrosines on the cytokine receptor, as well as the phosphotyrosine on the activation lip of JAK (Lodish et al.). This prevents STATs from binding the receptor and JAKs from phosphorylating STAT (Lodish et al.). SOCS proteins also have a SOCS box that can recruit E3 ubiquitin ligase, which can ubiquitinate JAK2 upon binding causing its degradation within a proteasome (Lodish et al.).

Protein inhibitor of activated STAT (PIAS) is another common regulator of STAT signaling (Heinrich et al.). PIAS acts by binding a STAT protein after it has been phosphorylated on Tyr 727 (Heinrich et al.). The exact mechanism of PIAS function on STAT is unclear (Heinrich et al.). However, PIAS has been known to demonstrate E3-

Small Ubiquitin-Like Modifier (SUMO) ligase activity, which could help relocate the STAT protein to another area of the nucleus to become inactive (Heinrich et al.).

1.13 Stat3

Stat3 is a member of the STAT family of transcription factors. This particular STAT protein was discovered in 1994 (Mogensen). This protein is 770 amino acids in length and the gene encoding this molecule can be found on chromosome 17q21 (Mogensen). Like other members of the STAT family, Stat3 has an N-terminal domain (1-130), a coiled-coil domain (130-320), a DNA binding domain (DBD, 320-465), a linker domain (465-585), an SH2 domain (585-688), and a C-terminal transactivation domain (688-770)(Holland et al.; Fagard et al.; Xu et al.). (Figure 3) Descriptions based on the structure of the protein list an N-terminal region (1-355) which includes the N-terminal domain and a portion of the DBD, a central area (355-555) with the other portion of the DBD, and a C-terminal domain (555-770) which includes the SH2 domain (Xu et al.). Stat3 activation can occur through a variety of cytokines and growth factors, including Interleukin (IL)-6 (Mogensen). (Figure 4) Stat3 has been shown to activate upon phosphorylation by Tyrosine Kinase (Tyk) 2, Jak1, Jak2, and Jak3 based on what ligand/receptor combination is used (Rebe et al.). Dimerization occurs once the K685 is acetylated and the Y705/S727 is phosphorylated (Xu et al.). Upon activation and dimerization, Stat3 most often forms a homodimer but can also form a heterodimer with Stat1 or Stat5 (Mogensen). Stat3 then undergoes further modification through phosphorylation of Tyr 727, acetylation, and methylation (Mogensen). Stat3 then can enter the nucleus and bind promoters for genes such as Socs3, Fosl1, Jun, and Jak2 (Dauer et al.). Several residues in the DBD - E434, E435, V461, V462, V463 – are needed in order to bind the SIE in the promoter sequence (Xu et al.). Once Stat3 has successfully induced its target genes, it is dephosphorylated and sent back into the cytoplasm to be recycled (Mogensen).

1.14 Stat3 in Hyper-IgE Syndrome (HIES)

1.14.1 HIES Characterization

Hyper-immunoglobulin E syndrome (HIES) is a disorder commonly associated with Stat3. There are two different types of HIES, Type 1 and Type 2 (Minegishi and Karasuyama). Type 1 is caused by mutations in Stat3 whilst Type 2 is characterized by a null mutation in Tyk2 (Minegishi and Karasuyama). Both types have similar issues in that cytokine signaling is significantly impaired, leading to many problems with the immune system – particularly from T-helper type 17 cells – and several other cellular functions (Minegishi and Karasuyama). Type 1 HIES, more commonly referred to as autosomal dominant hyper-immunoglobulin E syndrome (AD-HIES), or Job's Syndrome, is a disorder in which there is an autosomal dominant mutation of the Stat3 gene in humans. Patients with AD-HIES have several major issues including elevated IgE levels, connective tissue abnormalities, and skeletal development abnormalities (Sowerwine et al.). Some studies have shown that many patients with AD-HIES have osteopenic or osteoporotic phenotypes (Sowerwine et al.). There is evidence these phenotypes occur due to an increase in osteoclast activity (Sowerwine et al.). Stat3 is activated in the presence of factors such as IL-6, IL-10, IL-11, IL-17, IL-21, and IL-22, so when Stat3 is not functioning correctly, all of these cellular pathways are negatively affected (Mogensen). The wide range of issues caused by Stat3 mutations demonstrates the breadth of Stat3's effect on different cell types. Stat3 clearly has an important role to play in many tissues of the body, including bone.

1.14.2 HIES Mutations

When the link between AD-HIES and Stat3 was made, mutations were found at several different amino acids including R382, F384, R423, and V463 in the DBD and V637 in the SH2 domain (Holland et al.). Each of these amino acid changes has multiple mutations that can occur that influence them (Holland et al.). These mutations in Stat3 can either be missense or in-frame deletions, and they do primarily occur in the DBD and SH2 domains (Mogensen). They have occasionally been shown to occur in the transactivation domain as well (Giacomelli et al.). The mutations that occur within the DBD prevents binding to the promoter regions of the target genes Stat3 affects through

SIE, which impairs the transcription of several critical factors (Xu et al.). These mutations have the potential to cause changes in several different amino acids including R382Q, R382W or V463Δ which are critical for DBD binding to the promoter sequence (Xu et al.). SH2 mutations inhibit the initial activation step where Stat3 needs to bind to the receptor in order to be phosphorylated by the Jak protein (Giacomelli et al.). Some amino acid changes caused by these mutations are V637M and M660R (Giacomelli et al.).

1.15 Stat3 Effect on Bone

Many studies have been done that demonstrate that Stat3 has an effect on bone morphology and development. The extent of this effect and whether the effect is positive or negative is still unclear. Many studies show what appear to be conflicting results in this respect. HIES patients have a mutation in Stat3 that typically causes a net loss in bone mass, which might indicate that Stat3 has an overall positive effect on bone mass essentially preventing bone from being broken down too much. However, the answer might not be as simple as this. There are several researchers who have studied and are currently studying different ways Stat3 could affect bone mass.

One study that also used an *in vivo* system incorporated an α1(I)-collagen Cre-LoxP to conditionally knock out Stat3 in osteoblasts (Itoh et al.). They found that transgenic mice tended to have osteoporotic phenotypes, suggesting the osteoblast function was impaired when Stat3 was deficient in osteoblasts (Itoh et al.). The main conclusion is that Stat3 positively regulates osteoblast differentiation to support bone formation, similar to our findings (Itoh et al.).

Another study confirmed the involvement of Stat3 in osteoblast differentiation by transfecting cells with either constitutively active or dominant negative Stat3 (Nicolaidou et al.). demonstrated that Stat3 is essential for causing osteoblast differentiation from mesenchymal stem cells (Nicolaidou et al.). This was an *in vitro* study, so they were unable to assess how osteoblast activity was affected in any way. However, this study demonstrated the vital role Stat3 plays in causing osteoblasts to differentiate from mesenchymal stem cells. Stat3 studies in relation to osteoblasts seem to be in agreement that Stat3 has a positive effect on osteoblasts, be it by assisting in their commitment,

differentiation, or function. There is currently not much information available on the extent of this effect and how bone mass is affected by it.

One lab did study the effect of Stat3 on osteoclasts *in vivo* and *in vitro* (Z. Zhang et al.). They began by conditionally knocking out Stat3 in hematopoietic stem cells (HSCs) of 3-4 week old mice using Tie2-Cre, which likely did not affect osteoblast cells but affected osteoclasts (Z. Zhang et al.). This Cre is not specific for osteoclasts, so may have also knocked Stat3 out in other cell types produced from HSCs. From this experiment, they found increased osteoporosis based on decreased trabecular/cortical bone mass that was likely caused by increased osteoclast precursor/osteoclast number (Z. Zhang et al.). Cells from these mice were cultured *in vitro* for further testing (Z. Zhang et al.). They analyzed c-Fos mRNA and protein levels in osteoclast precursor cells and showed these levels greatly increase in the absence of Stat3 (Z. Zhang et al.). One conclusion of this study is that because c-Fos is needed for osteoclast differentiation, Stat3 is a negative regulator of osteoclastogenesis due to its apparent inhibitory effect on c-Fos (Z. Zhang et al.).

Another study was done to elucidate the role of Stat3 in osteoclastogenesis using a similar model to ours. The researchers in this study cultured mouse osteoclast precursor RAW264.7 cells with M-CSF, RANKL, and varying concentrations of JAK inhibitor AG490 (Li et al.). They found that the addition of AG490 inhibited osteoclast formation compared to cells without (Li et al.). When they added only RANKL with AG490, they saw a decrease in cell surface receptor RANK (Li et al.). The general conclusion of this paper is that AG490 inhibits osteoclastogenesis (Li et al.). From this, they believe that Stat3 must be a positive regulator of osteoclastogenesis (Li et al.). They also saw that adding AG490 to RAW264.7 cells with or without RANKL inhibited cell growth and proliferation, indicating Stat3 could be important for maintaining the cell population (Li et al.). One issue with this study is that JAK inhibition is not simply Stat3 inhibition. JAK is influenced by many different cytokines and growth factors and affects many different cellular pathways that do not directly involve Stat3. The experimental design used in this paper does not have the same level of clinical relevance to HIES as studies that directly use Stat3 as their target. This study did demonstrate that because AG490 inhibits RANKL

effects, JAK must be downstream of RANKL (Li et al.). Essentially, AG490 inhibits RANKL-induced activation of Stat3 (Li et al.).

A study that used human embryonic kidney HEK293 cells, interestingly enough, shed some light on whether Stat3 could have a positive or negative effect on osteoclastogenesis (Wei et al.). Their focus was on the interaction of TRAF6, an important protein activated by RANKL signaling, and Stat3 (Wei et al.). When they used an antibody to precipitate Stat3, they found that TRAF6 co-precipitated, demonstrating the two proteins interact (Wei et al.). Through further analysis, they were able to demonstrate that TRAF6 interacts with Stat3 to ubiquitinate this protein as a target for destruction (Wei et al.). One could speculate that because TRAF6 is needed to induce osteoclastogenesis and it inhibits Stat3, the latter could be important in down-regulating osteoclastogenesis.

1.16 Research Goals

Currently, there is research that promotes the idea Stat3 has an effect on bone development and morphology. Some of the research seems to be contradictory in that there is not a consensus on whether Stat3 has a positive or negative effect on bone development. Currently, most researchers seem to agree that Stat3 has an inhibitory effect on osteoclastogenesis and osteoclast function and a promotional effect on osteoblastogenesis and osteoblast function, but the mechanisms are still not well understood. Many researchers have even suggested that Stat3 has a positive role in osteoclastogenesis, causing an overall catabolic effect on the skeleton.

Our lab created Stat3 conditional knockout mice in the osteoblasts of developing mice with an Osterix promoter to further explore the role of Stat3 in osteoblasts. Osterix is an important protein that assists in differentiating a pre-osteoblast to a fully functional osteoblast. Because of this, the Osterix promoter was used specifically to knock out Stat3 in pre-osteoblasts in an effort to understand how osteoblasts are affected by Stat3 deletion. We hypothesize that when Stat3 is not present in fully developed osteoblasts, there are deficits in the developing skeleton.

Stat3 was also knocked down in pre-osteoclasts specifically to understand how osteoclast differentiation and function are affected by a deficiency of Stat3. To test how differentiation and function might be affected, RANKL was added to a control and a Stat3 knockdown group. RANKL is used to differentiate osteoclasts, so this would cause an upregulation in genes important in osteoclastogenesis and osteoclast function. If Stat3 affected these genes, an upregulation or downregulation of said genes would be visualized upon siRNA knockdown. For similar reasons, Stat3 overexpression was performed to test if a similar pattern would be seen as with siRNA knockdown. For instance, if a gene was upregulated when Stat3 was knocked down, the same gene should have been downregulated when Stat3 was overexpressed. Genes that are known to be important in differentiation and function were chosen in order to test how important Stat3 is in bone resorption. Our findings show that Stat3 downregulates genes important for osteoclast differentiation and function, resulting in a positive effect on bone mass. Our hypothesis is that Stat3 does have a negative effect on osteoclastogenesis and a positive effect on osteoblastogenesis, thus providing an overall anabolic effect on skeletal development. The goal of this study is to test this hypothesis by elucidating what roles Stat3 has on bone development based on how it affects osteoclasts in vivo using a cKO system and in vitro by using siRNA knockdown and an overexpression construct of Stat3, and how it affects osteoblasts in vivo using a cKO system in early osteoblast differentiation.

CHAPTER 2. MATERIALS AND METHODS

2.1 *In vivo* Mouse Study

2.1.1 Experimental Mice

In order to knock out Stat3 in osteoblasts of experimental mice, a cre-loxP recombinase system was used. The Osterix promoter was used ensuring Stat3 was only knocked out in early osteoblasts. LoxP flanked the 18-20 exons on the Stat3 gene that are responsible for encoding the SH2 region, which is needed for activation.

2.1.2 Breeding Scheme

Cre+ mice were bred with $LoxP^{+/+}$ mice to produce the F1 generation. Of these, Cre+ mice were saved for further use. Pups that were $LoxP^{+/+}$ were used as experimental animals and $LoxP^{-/-}$ were used as controls. $LoxP^{+/-}$ were used for breeder pairs in order to continue obtaining experimental and control mice.

2.1.3 Genotyping

Mice were genotyped at 3 weeks old. A 1-2 mm piece at the end of their tails was removed and placed in a 1.5 mL microfuge tube. In each tube, 100 uL lysis buffer (50 mM Tris, 50 mF KCL, 2.5 mM EDTA, 0.4% NP-40, 0.45% Tween-40) and 2 uL Proteinase K (0.4 mg/mL) were added and the tubes were placed in a 55^{o}C water bath overnight. The next morning, the tubes were centrifuged for 30 seconds at 13.2 rpm and placed in a 95^{o}C heat block for 10 minutes. Afterwards, 100 uL RNase DNase-free water was added to each tube.

A PCR mix was assembled using 12.5 uL REDTaq ReadyMix (Sigma-Aldrich, St. Louis, MO, USA), 5.5 uL PCR water, 0.5 uL (0.5 mM) forward primer, and 0.5 uL (0.5 mM) reverse primer in each 0.2 mL PCR reaction tube. Finally, 1.5 uL mouse DNA was added to the tube for a total of 20.5 uL. Two sets of primers were used to genotype mice – Stat3 and Osterix-Cre. The Stat3 primer sequences were as follows: forward – 5'-ATT GGA ACC TGG GAC CAA GTG G-3' and reverse – 5'-ACATGT ACT TAC AGG GTG TGT GC-3'. The Osterix-Cre primer sequences were as follows: forward – 5'- CTC

TTC ATG AGG AGG ACC CT -3’ and reverse – 5’- GCC AGG CAG GTG CCT GGA CAT -3’. The tubes were placed in an Eppendorf Thermal Cycler and run for 40 cycles. After amplification, samples were loaded into a 2.5% agarose gel with 1x SYBR safe DNA stain (Life Technologies Corporation, Carlsbad, CA, USA) alongside a 100 bp ladder. Gels were imaged using a Typhoon FLA 9500 Scanner.

For the Stat3 LoxP primers, a band at 520 indicated $Stat3^{flox/flox}$ and a band at 480 indicated $Stat3^{+/+}$. The presence of both bands indicated a heterozygous genotype. Cre positive mice were identified by the presence of a 615 bp band. If the mice were Cre negative, no band appeared. The Cre that was used is only found in pre-osteoblast cells, so this system ensured that Stat3 was conditionally knocked out in pre-osteoblasts.

2.1.4 Sacrificing

$Stat3^{flox/flox}$ and $Stat3^{+/+}$ pups were euthanized at 8 weeks. One week prior to euthanization, mice were injected with calcein (green fluorochrome label, 30 mg/kg body weight) intraperitoneally. Two days prior to euthanization, mice were injected with alizarin (red fluorochrome label, 50 mg/kg body weight). Mice were sacrificed by placing them in a carbon dioxide chamber until all visible signs of breathing ceased for at least one minute. The mice were then removed from the chamber and underwent cervical dislocation to ensure their deaths. After sacrificing the mice, several different tissues were harvested including the left and right femur, left and right tibia, lumbar, and tail snip. The left femur was stripped of soft tissue and wrapped in 0.85% saline soaked gauze and stored in a -20°C freezer. The right femur was stripped of soft tissue and placed in a small jar filled with 10% neutral buffered formalin and placed in a 4°C refrigerator. The following day, the formalin was removed and replaced with 70% ethanol. The left and right tibia were stripped of soft tissue and placed in individual 1.5 mL microfuge tubes and stored in a -80°C freezer. The lumbar vertebrae was stripped of soft tissue and wrapped in 0.85% saline soaked gauze to be stored in a -20°C freezer. Finally, a 1-2 mm piece of tail was removed to confirm the genotype and prepared as previously described.

2.1.5 Bone Mineral Density and Content

Bone mineral density (BMD, g/cm^2) and bone mineral content (BMC, g) were measured in the left femurs of experimental and control mice. These femurs were thawed at room temperature from -20°C and placed in a peripheral dual-energy X-ray absorptiometry (pDXA, PIXImus II, GE-Lunar Co.) machine that calculated BMD and BMC.

2.1.6 Micro-Computed Tomography (CT)

Left femurs were analyzed using micro-CT. They were first thawed at room temperature from -20°C and wrapped in Parafilm. Femurs were stabilized with Styrofoam and placed in the machine (SkyScan 1176, Bruker-microCT, Kontich, Belgium). The following parameters were set prior to scanning: voltage: 60kV, resolution: 9 μm, binning mode: 2K, filter: Al 0.5 mm, rotation step: 0.9°, and averaging frame: 2.

2.1.7 Histology

Excess tissue was trimmed off the right femurs and they were measured lengthwise. A pencil marked was placed around the center of the bone shaft and a bone saw was used to cut the bone approximately 1 millimeter distal to the pencil marking. A small portion of bone was shaved off the distal end. Both bone fragments were placed in small chambers and set in a large beaker of ethanol that was changed every 2-8 hours in gradients before being cleared in xylenes for 2-8 hours. Next, methyl methacrylate (MMA) and 100% ethanol were used to infiltrate the femurs for another 2-8 hours before being changed to pure MMA for another 2-8 hours. The femurs were then added to unpolymerized MMA and 4% dibutyl phthalate for less than a week before being embedded.

2.1.7.1 Slide Preparation of Midshaft

The midshaft portion of the femurs were fixed in a mixture of MMA, 4% dibutyl phthalate, and 0.25% Perkadox 16 inside a glass vial. After 2 hours inside of a vacuum, the vials were capped. These vials were set in a 4°C refrigerator overnight and allowed to polymerize at room temperature the following day. Vial caps were removed and a hammer was used to break off the glass from the polymerized samples. A wire saw was used to shave 4 different 40-45um cross sections off the midshaft of each femur to be

fixed in slides. These sections were placed onto a drop of Eukitt on a slide and pressed down until they made contact with the slide. A small piece of paper towel was set on top of the section and another slide was placed on top of the paper towel. A binder clip was used to hold the pieces together overnight. The next day, the top slide and paper towel were removed. Several drops of xylenes-thinned Eukitt (2 parts Eukitt; 1 part xylenes) were placed on top of the slide until the section was completely covered. These slides were allowed to dry overnight. The following day, sections were ground down to a thickness of 20-40 um by placing them section-down on water-covered 600 grit wet/dry silicon carbide sandpaper (LECO) and gently moved across the paper in a figure-8 motion. After these sections were dried, the slides were dipped several times into a beaker of xylenes. Excess xylenes was wiped off the slide and a drop of Eukitt was placed on the section, followed by a glass cover slip.

2.1.7.2 Slide Preparation of Distal

Distal femurs were embedded in vials in a mixture of MMA, 4% dibutyl phthalate, and 0.25% Perkadox 16. After 2 hours inside of a vacuum, the vials were capped. These vials were set in a 4°C refrigerator overnight and allowed to polymerize at room temperature the following day. A bone saw and dental model trimmer were used to trim off excess plastic before sections were cut. Five longitudinal sections 4 um thick were cut from each right femur with a tungsten-carbide knife fitted in a rotary microtome. Two of these sections were used to analyze fluorescent labels, one was used for TRAP staining for osteoclasts, one was used for VKM staining for osteoblasts, and the final section was used as a spare.

2.1.8 Dynamic Histomorphometry

Midshaft cross sections were used to calculate cortical parameters. Sections were analyzed at 200x under a fluorescent microscope. Periosteal and endosteal surfaces were traced along with single and double labels of calcein and alizarin. Using these measurements, MS/BS, MAR, and BFR/BS were calculated.

Distal longitudinal sections were used to calculate trabecular parameters. Unstained sections were used to measure calcein and alizarin labels, as well as the bone surface.

Measurements were taken approximately 0.5mm proximal to the growth plate centered form the periosteal surface. The tissue area measured was 0.4mm^2.

2.2 Osteoclast Preparation

2.2.1 Cell Culture

2.2.1.1 Stat3 Suppression

One hundred thousand RAW 264.7 cells were seeded in 5 mL antibiotic-free medium (1000 mL MEM-alpha in 100 mL FCS) in four different 6 cm petri dishes [2 controls (NC, siRNA) and 2 RANKLs (NC, siRNA)]. The plates were incubated 24 hours before the addition of siRNA. Stat3 Silencer Select siRNA was used to knock down Stat3 and New NC2 Custom Select siRNA was used as a negative control (Ambion). The siRNA was prepared by centrifuging the vial for 45 seconds in a mini-centrifuge. Enough water, in this case 250 uL was added for a final concentration of 20 uM. Two separate 1.5 mL RNAse-free tubes were prepared by adding 10 uL Lipofectamin RNAiMax to one and 6.25 uL siRNA to the other. In both tubes, 500 uL OPTI-MEM was added and the tubes were incubated for 5 minutes in a Bio Safety Cabinet. After incubation, they were added together and incubated for an additional 20 minutes in a Bio Safety Cabinet. During incubation, the medium was removed from each of the dishes and replaced with 4 mL fresh antibiotic-free medium. After the second incubation, the mixture was added to 2 of the dishes for a final siRNA concentration of 25 nM. The plates were incubated for 6 or 24 hours and the medium was changed with 5 mL 10% FBS 1% antibiotic medium. RANKL at a concentration of 10 ug/mL was added beforehand to PBS 0.1% BSA and stored at -20^o freezer until use. After the medium was changed, 25 uL of the RANKL solution was added to a dish with siRNA and a dish without siRNA. The other dishes were given a control of 25 uL PBS 0.1% BSA. After 24 hours, the cells were harvested.

2.2.1.2 Stat3 Overexpression

One hundred thousand RAW 264.7 cells were seeded in 5 mL antibiotic-free medium (1000 mL MEM-alpha in 100 mL FCS) in four different 6 cm petri dishes [2 controls (NC, construct) and 2 RANKLs (NC, construct)]. The plates were incubated 24 hours

before the addition of the plasmid. Stat3C-Flag pRc/CMV was used to overexpress Stat3 and was a gift from Jim Darnell (Addgene plasmid #8722). (Figure 5) An empty CMV plasmid was used as a negative control. Two separate 1.5 mL RNAse-free tubes were prepared by adding 11 uL Lipofectamine LTX to one and 6.9 uL construct (5.5 ug) or 9.2 empty plasmid (5.5 ug) and 5.5 uL PLUS reagent to the other (Thermo Fisher Scientific). In both tubes, 250 uL OPTI-MEM was added and the tubes were incubated for 5 minutes in a Bio Safety Cabinet. After incubation, they were added together and incubated for an additional 20 minutes in a Bio Safety Cabinet. During incubation, the medium was removed from each of the dishes and replaced with 4.5 mL fresh antibiotic-free medium. After the second incubation, the mixture was added to 2 of the dishes. The plates were incubated for 6 hours and the medium was changed with 5 mL 10% FBS 1% antibiotic medium. RANKL at a concentration of 10 ug/mL was added beforehand to PBS 0.1% BSA and stored at -20^{o} freezer until use. After the medium was changed, 25 uL of the RANKL solution was added to a dish with the construct and a dish the empty plasmid. The other dishes were given a control of 25 uL PBS 0.1% BSA. After 24 hours, the cells were harvested.

2.2.2 Protein Collection

Radioimmunoprecipitation assay (RIPA) lysis buffer was prepared in a 15 mL conical on ice by mixing together 500 uL RIPA, 5 uL PMSF, 5 uL Na Ortho, 17.5 uL protease inhibitor, and 20 uL phosphatase inhibitor per dish. The medium was aspirated from the dishes and the cells were washed 3x with 5 mL PBS. After the last aliquot of PBS was aspirated from the dishes, 500 uL RIPA buffer was added to each one. Plates were kept on ice for 5 minutes completely horizontally. The dishes were then scraped and the cells were transferred to their own 1.5 mL tube in ice. The cells were sonicated on ice for 25 seconds per tube. These were then centrifuged at 4^{o}C for 10 minutes on 13,200 rpm. The supernatant was transferred to separate tubes and placed on ice or stored in the -80^{o} freezer.

2.2.3 Calculating Protein Concentration

BCA was prepared in a 15 mL conical by mixing 400 uL BCA Reagent A with 8 uL BCA Reagent B per sample. The protein samples were microfuged and gently mixed with a pipetman. For each sample, 10 uL of protein was added to two different wells in a 96-well plate. BSA protein standards in concentrations of 0, 0.125, 0.25, 0.5, 1, and 2 mg/mL were included in the samples measured. Afterwards, 200 uL of the BCA mixture was added to each well sample. The plate was put in a shaker for 20 seconds and immediately covered in film and wrapped in aluminum foil. The plate was then incubated for 30 minutes in the incubator and 30 minutes at room temperature. The foil was quickly removed and any bubbles were popped using a pipetman before the plate was placed in the machine to measure the concentrations.

2.2.4 RNA Collection

For each sample, 500 uL RLT Plus buffer and 5 uL 2-mercaptoethanol was added in a 15 mL conical and vortexed. The medium was aspirated from the cell culture dish and 350 uL of the mixture was added. The cells were scraped thoroughly and transferred to a Qiashredder tube, which was centrifuged for 2 minutes at 13,200 rpm. The lysate was removed from the Qiashredder and added to the gDNA Eliminator spin column and centrifuged for 0.5 minutes on 10,000 rpm. After centrifugation, 350 uL 70% EtOH was added to the lysate, which was then transferred to an RNeasy spin column and centrifuged at 0.5 minutes on 10,000 rpm. The lysate was then discarded and 700 uL RW1 buffer was added to the tube over a filter. This was centrifuged at 0.5 minutes on 10,000 rpm and the lysate was discarded. After, 500 uL RPE buffer was added to the tube over a filter and the tube was centrifuged for 0.5 minutes on 10,000 rpm. The lysate was again discarded and another 500 uL aliquot of RPE Buffer was added, and the tube was centrifuged at 2 minutes on 10,000 rpm. The lysate was discarded and the filter was placed over a new tube and centrifuged for 4 minutes on 13,200 rpm. The filter was then added to another clean tube and 100 uL RNAse-free water was poured over the filter. The tube was then centrifuged for 1 minute on 10,000 rpm. The filter was removed and the lysate was gently mixed with a pipetman. The machine was first cleaned, then blanked,

with RNase-free water. For each sample, 1.5 uL lysate was added to the machine and the RNA concentration was measured.

2.2.5 RT-PCR

RT-PCR mix was prepared in a 200 uL microfuge tube by adding 2 uL 10x RT buffer, 0.8 uL 25x dNTP mix (100mM), 2 uL 10x RT random primers, and 1 uL MultiScribe Reverse Transcriptase per sample. The proper volume equaling 1000 ng from each RNA sample was added to the RT mixture. Water was added to the mixture so that the volume of lysate + water equaled 14.2 uL, and the total volume in the tube was 20 uL. The samples were then placed in the thermal cycler to make cDNA. Once the samples were finished, 180 uL of water was added to each tube and the contents were transferred to 1.5 mL tubes for storage.

2.2.6 qPCR

qPCR mix was prepared in a 1.5 mL microfuge tube by adding 10 uL 2x Master Mix, 1 uL forward primer, 1 uL reverse primer, 6 uL water, and 2 uL cDNA per sample. In a 96-well plate, 2 uL of each sample (including water blank) was added to 2 different wells per transcript. In each well containing a sample, 18 uL of qPCR mix was added. The plate was then centrifuged for 1 minute on 1800 rpm. Finally, the plate was placed in a PCR-7500 Fast system for approximately 90 minutes. This protocol was used on 40 different primers. (Table 1)

2.2.7 Western Blot

Protein samples were defrosted, centrifuged, and mixed with a pipetman before being placed on ice. SDS buffer was diluted 4x in each sample by adding 5 uL SDS buffer to 1.5 mL centrifuge tubes and adding 15 uL sample to each tube. Additional tubes were made with 5 uL SDS buffer and 15 uL of a molecular weight standard. Once these mixtures were prepared, they were placed on a 100^{o}C heat block for 5 minutes. The samples were then centrifuged for 1 minute on 13,200 rpm. Gel boxes were assembled with 10% 10 well premade gels. Loading buffer was added to the boxes and the bubbles were broken apart. Each of the wells was washed out with a pipetman to remove debris. Each of the samples was gently mixed with a pipetman, careful to avoid producing

bubbles. First, 10 uL of the molecular weight ladder was added to the first and last wells. Then, varying volumes of each protein were added to the rest of the wells, based on what concentrations were measured previously. The gel was run at 100 V for 10 minutes and 150 V for 40-50 minutes, until the dye front reached the bottom of the gel. PVDF membranes for each gel were placed in MeOH for 10 minutes. Blotting paper, 2 for each membrane, was placed in a separate container which was then filled with transfer buffer (3.03 g Tris, 14.4 g glycine, 787 mL water, 200 mL MeOH). At the end of the 10 minutes, the MeOH was changed out for transfer buffer. When the gel finished running, it was removed from the gel box and cut carefully around the edges and in the upper left corner. A piece of blotting paper was placed on the transfer machine and a membrane was placed on top of the blotter. The gel was then carefully placed on top of the membrane and covered with another piece of blotting paper and pressed down with a 15 mL conical. The machine was turned on for varying times depending on the protein, from 30 minutes for smaller proteins to 55 minutes for larger proteins. Once the proteins transferred to the membrane, the membrane was removed and unnecessary pieces were cut away. The membrane was placed in blocking buffer (1 g blocking powder (non-fat dry milk), 50 mL PBS/Tween (1000 mL 1x PBS + 500 uL Tween 20)) and placed on a shaker at 35 rotations per minute for 1 hour. During this time, Parafilm was placed on large plate. To prepare the primary antibody, 1.5 mL PBS/Tween was added to a 1.5 mL centrifuge tube and mixed with 1.5 uL antibody to tube. Antibodies used include the following: b-actin (Sigma-Aldrich), p-Stat3 (Ser727, Santa Cruz), NFATc1 (Santa Cruz), c-Fos (Santa Cruz), and Cathepsin K (Santa Cruz). Once the membrane finished shaking, half of the antibody mixture was added onto the Parafilm and the membrane was placed face down in the antibody. The rest of the mixture was placed on top of the membrane and allowed to sit for 1 hour. After this period was over, the membrane was placed in PBS/Tween and put on a shaker at 65 rotations per minute for 2 minutes. The PBS/Tween was changed and the membrane was put back on the shaker for 2, 15, 5, 5, and 5 minutes with new PBS/Tween each time. To make the secondary antibody, 1.5 mL PBS/Tween was added to a 1.5 mL centrifuge tube and mixed with 0.75 uL 2^{o} antibody (different antibodies for different primaries) to tube for 2000x dilution. Half of this mixture was added to the Parafilm and the membrane was placed on top. The rest of mixture was added to the

membrane and allowed to sit for 45 minutes. After this period, the membrane was placed in PBS/Tween for 2 minutes. The PBS/Tween was changed and the membrane was placed back on the shaker for 2, 15, 5, 5, 5, and 5 minutes with new PBS/Tween each time. The Parafilm was changed out for a fresh piece and Saran wrap was laid flat on table. To prepare the developing solution, 750 uL each of Peroxide Buffer and Luminol/Enhancer was added to a 1.5 mL tube and shaken. Half of this mixture was added to the Parafilm. The membrane was placed on top and the rest of the mixture was added before allowing the membrane to set for 5 minutes. The membrane was dried on a paper towel by placing the membrane between 2 pieces and gently pressing. The membrane was then wrapped in the Saran wrap and placed in the LAS-3000 so pictures could be taken.

2.2.8 Microarray

Cells were prepared as previously described. Three different sets of plates were used to culture the following groups of cells: non-specific siRNA with no RANKL, Stat3 siRNA with no RANKL, non-specific siRNA with RANKL, and Stat3 siRNA with RANKL. RNA was collected from these triplicated groups and sent off to be analyzed. The data obtained was analyzed and grouped. Both RANKL groups were compared and genes with a significant change ($p < 0.05$) and with a 1.2 fold change were further analyzed using qPCR. All of the genes found to have differential regulation between the RANKL groups were entered into the Kyto Encyclopedia of Genes and Genomes (KEGG) pathway analysis to find possible pathways these genes are involved in.

2.2.9 TRAP Staining

RAW264.7 cells were seeded $1x10^5$ cells per 5cm dish in 5ml MEM-a PS(-)FCS10%. Cells were transfected the following day with Stat3 siRNA 0.5nM in each dish. Exactly 24h after transfection, cells were reseeded onto a 96-well plate. Approximately 5000 cells were seeded into each well and 200uL of MEM-a PS(+)FCS10% was added. After 8h, 1 uL PBS 0.1％BSA was added to half the siRNA groups and half the control groups, and 1uL 10ug/mL RANKL was added to half the siRNA groups and half the control groups for a final concentration of 50ug/mL. These cells were incubated the following

day in a 37^{o} incubator. The next day, the medium was changed again and more PBS 0.1% BSA and RANKL were added to their respective wells. At 72-96h, the cells were observed for floating. Before they dissociated, they were stained with TRAP.

2.3 Statistical Analysis

All data are reported as mean ± standard error of the mean. Groups were compared to test for significance using a 2 sample t-test with Excel function =TTEST(array1,array2,2,2). Significance was assumed if $p < 0.05$ and high significance was assumed if $p < 0.01$. Significant outliers were removed from the sample using Grubbs' test through the GraphPad calculator.

CHAPTER 3. RESULTS

3.1 OSX-Cre Stat3-LoxP cKO 8-Week Mouse Models

3.1.1 Phenotypes

Using the Osterix-Cre Stat3-LoxP breeding scheme, 7 male WT, 4 male KO, 8 female WT, and 9 female KO mice were generated. There was a 32.41% highly significant decrease in weight between the WT and KO males ($p < 0.01$) as well as a 19.68% highly significant decrease in weight between the WT and KO females ($p < 0.01$). The average body weights for each mouse type with standard deviation are as follows: WT male 19.16 ± 2.25g, cKO male 12.95 ± 3.01g, WT female 16.06 ± 1.68g, cKO female 12.9 ± 2.35g. (Figure 6) These weights were reflected in the notable size difference between the WT and cKO mice as well. (Figure 7)

There was a highly significant decrease in femur length from WT males to cKO males ($p < 0.05$) as well as from WT females to cKO females ($p < 0.01$). (Figure 8) The average femur length for WT males was 14.0 ± 0.4 mm and the average femur length for cKO males was 11.4 ± 0.8 mm, which resulted in an 18.4% decrease. The average femur length for WT females was 13.4 ± 0.9 mm and the average femur length for cKO females was 12 ± 1 mm, which resulted in a 13.3% decrease. (Figure 9)

Measurements of bone mineral density revealed a slight decrease from the WT males to the cKO males that did not reach significance. The BMD also decreased from WT females to cKO females reaching signifance ($p < 0.05$). WT males had a BMD of 0.040 ± 0.003 g/cm^2 while cKO males had a BMD of 0.032 ± 0.007 g/cm^2 resulting in an 18.3% decrease. WT females had a BMD of 0.038 ± 0.003 g/cm^2 while cKO females had a BMD of 0.034 ± 0.005 g/cm^2 resulting in an 11.1% decrease. (Figure 10)

Measurement of bone mineral content (BMC) revealed a significant decrease from the WT males to the cKO males ($p < 0.05$). There was also a significant decrease from the WT females to the cKO females ($p < 0.05$). WT males had a BMC of 0.014 ± 0.003 g while the cKO males had a BMC of 0.008 ± 0.005 g, resulting in a 45.1% decrease. WT

females had a BMC of 0.012 ± 0.003 g while the cKO females had a BMC of 0.008 ± 0.004 g resulting in a 33.8% decrease. (Figure 11)

3.1.2 Micro-CT Analysis

Micro CT analysis revealed a metaphyseal defect that appeared in cKO males and females in relation to their WT counterparts. These femurs appeared shorter with a bulging out at the metaphysis. (Figure 12)

In the micro CT analysis of the distal region of the femur of trabecular bone, no significant differences were observed in any of the parameters that were measured, which included tissue volume, bone volume, bone volume over tissue volume, tissue surface, bone surface, bone surface over bone volume, and bone surface over tissue volume. Bone surface over bone volume exhibited somewhat of a decrease between WT and cKO males, but did not fully reach significance.

In the micro-CT analysis of cortical bone in the midshaft region of 8-week experimental mice, both the male and female mice showed a significant decrease from the WT to the cKO in tissue volume. (Figure 13) The male decrease was highly significant going from 12 ± 2 mm^3 in the WT to 7 ± 2 mm^3 in the cKO. The female significant decrease was 11 ± 2 mm^3 in the WT to 8 ± 3 mm^3 in the cKO. There was a similar pattern in bone volume where WT males had 10 ± 2 mm^3 and cKO males had 6 ± 2 mm^3, giving a highly significant decrease. WT females had 9 ± 2 mm^3 where cKO females had 7 ± 2 mm^3, giving a significant decrease in bone volume. (Figure 14) There was, however, no significant change seen in percentage of bone volume over tissue volume from WT to cKO in either the males or the females. (Figure 15) No significant change was seen in these groups for tissue surface either. There was a slight decrease from WT males to cKO males and a slight increase from WT females to cKO females, but neither reached significance. (Figure 16) cKO males showed a significant decrease in bone surface area compared to the WT males while there was no change in females. WT males had a bone surface area of 350 ± 60 mm^2 compared to the cKO that had a bone surface area of 260 ± 60 mm^2. The same pattern was seen in bone surface perimeter where WT males had bone surface perimeter of 240 ± 40 mm and cKO males had a bone surface perimeter of 180 ±

40 mm, giving a significant decrease. (Figure 17) Bone surface over bone volume was highly significantly increased from the WT males to the cKO males as well as from the WT females to the cKO females. WT males had a BS/BV of 34 ± 4 mm^{-1} while cKO males had a BS/BV of 48 ±4 mm^{-1}. (Figure 18) WT females had a BS/BV of 33 ± 4 mm^{-1} while cKO females had a BS/BV of 47 ± 9 mm^{-1}.

3.1.3 Dynamic Histomorphometry Measurements

In the measurement of the calcein and alizarin labels of the trabecular distal region of the femur, a significant increase in MS/BS was seen in female cKO mice compared to the control. (Figure 19) cKO females had 49 ± 2% MS/BS while WT females had 40 ± 3%. There was no significant difference in males for this parameter. Both the MAR and BFR/BS rates yielded no significant differences in either the males or the females.

In measuring the labels in the cortical midshaft region, no significant differences were seen in the males. On the endocortical surface, there was a significant decrease in cKO females regarding MS/BS, MAR, and BFR/BS. (Figure 20) WT females had an MS/BS of 88 ± 3%, an MAR of 0.8 ± 0.1 um/day, and a BFR/BS of 250 ± 40 um^3/um^2/year, while cKO females had an MS/BS of 74 ± 4%, an MAR of 0.48 ± 0.5 um/day, and a BFR/BS of 130 ± 20 um^3/um^2/year. On the periosteal surface, there was a significant increase in cKO females regarding MAR and BFR/BS, but no significant difference in MS/BS. (Figure 21)

3.2 Osteoclast Stat3 siRNA and Overexpression

3.2.1 Microarray Analysis

The microarray performed on the four different groups of RAW 264.7 cells with 24 hour RANKL stimulation in triplicate revealed 296 genes that were significantly changed when Stat3 was knocked down compared to controls in RANKL. (Figure 22) Of these, 192 were significantly upregulated and 104 were significantly downregulated when Stat3 was knocked down in the RANKL groups compared to the control ($p < 0.05$). Of these, 41 genes were brought to light which in addition to having a p value less than 0.05 also had at least a 1.2 fold change between the two RANKL groups. Several of these genes

did not have information in the NCBI database and could not be further tested. However, 26 of the genes were analyzed for further confirmation using qPCR. Kyto Encyclopedia of Genes and Genomes (KEGG) pathway analysis of the microarray data revealed several cellular pathways these genes are involved in. (Table 2) Pathways that were of significance included Rheumatoid arthritis, Lysosome, Regulation of actin cytoskeleton, Collecting duct acid secretion, Amoebiasis, Phagosome, and Cell adhesion molecules (CAMs) ($p < 0.05$).

3.2.2 mRNA Expression Patterns

In the qPCR analysis of siRNA Stat3 knockdown samples stimulated with RANKL for 24h, Stat3 was shown to be sufficiently knocked down compared to controls. (Figure 23) Atp6v0d2, Bcar3, Cathepsin K, DEL1, DMPK, EEIG1, Hyal1, Ifi202b, Mapk11, Nfkbie, Nhedc2, OSCAR, Pdgfb, Rorc, Serpinb6b, Src, and 5-HTT qPCR confirmed the upregulation pattern seen in the microarray when Stat3 was knocked down with RANKL induction. (Figure 24) CD97, CEBPA, Gadd45g, HOX-a1, and Sla qPCR confirmed the downregulation pattern seen in the microarray when Stat3 was knocked down with RANKL induction. (Figure 25) COX1, Icam2, NOX2, and S1pr1 did not confirm microarray results, but none of their values reached significance. Out of 11 genes (Akt, AMPK, c-Fos, DC-STAMP, GLUT1, Mitf, NFATc1, PPARg, PU.1, TRAP, and UCP2) analyzed that were not found in the microarray results, only c-Fos was found to have a significant decrease in mRNA expression when Stat3 was knocked down.

3.2.3 Protein Production Patterns

3.2.3.1 Stat3 siRNA Knockdown

In the western blot analyses performed using the Stat3 siRNA, the b-actin control showed an even distribution of protein amounts. (Figure 26) p-Stat3 levels decreased in response to the siRNA in 6h and 24h of RANKL induction. (Figure 27) NFATc1 levels increased significantly at 6h and only slightly at 24h when Stat3 was knocked down compared to the control. (Figure 28) c-Fos levels slightly decreased at 6h and 24h in RANKL when Stat3 was knocked down, but this decrease was not significant. (Figure 29) Cathepsin K

levels increased significantly at 24h hours in RANKL when Stat3 was knocked down compared to the control group. (Figure 30)

3.2.3.2 Stat3 Overexpression Construct

In the western blot analyses performed using the Stat3 overexpression construct, the b-actin control showed an even distribution of protein amounts. (Figure 31) p-Stat3 levels increased significantly in response to the overexpression construct in each of these samples. (Figure 32) NFATc1 levels remained the same when Stat3 was overexpressed compared to the control. (Figure 33) c-Fos levels increased slightly though insignificantly at 6h in RANKL when Stat3 was overexpressed. (Figure 34)

3.2.4 TRAP Staining

In the TRAP staining done on RAW 264.7 cells stimulated with RANKL for 3-4 days, the number of multi-nucleated osteoclasts significantly increased when Stat3 siRNA was used compared to the negative control. (Figure 35 & Figure 36)

CHAPTER 4. DISCUSSION

4.1 Osterix Cre Stat3 KO in Osteoblasts

Both the male and female cKO mice exhibited a highly significant decrease in body weight as well as femur length in relation to their WT counterparts. cKO females had a significant decrease in bone mineral density compared to WT females. The same pattern was seen in males, but did not reach significance. Both male and female cKO mice had a significant decrease in bone mineral content compared to their WT counterparts as well. cKO mice also tended to be much smaller than the WT mice. There were very clear differences between WT and cKO mice phenotypically. Overall, there does not seem to be a large difference between the sexes in how Stat3 affects their pre-osteoblasts. Both the weight and femur length did seem to have a larger difference between the male WT and cKO than the female WT and cKO. It also seemed easier to breed female cKO than male cKO as there were more than twice as many female cKO obtained than male cKO. This could indicate that survival in the womb might have been more heavily affected in male cKO than in female cKO. Aside from experimental animal numbers, there is no further evidence of this effect based on the present study.

Micro-CT analysis of the 8-week mouse femurs revealed a metaphyseal defect in cKO mice of both sexes that appeared as a bulge in the metaphysis that was not present in WT mice. No difference between WT and cKO mice was observed in the trabecular analysis. Cortical bone analysis revealed several differences between WT and cKO mice. In male mice, a significant decrease was seen in tissue volume, bone volume, bone surface area, and bone surface perimeter from the WT to the cKO, and a significant increase was seen in bone surface over bone volume from the WT to the cKO. In female mice, a significant decrease was seen only in tissue volume and bone volume from the WT to the cKO, while a significant increase was seen in bone surface over bone volume from the WT to the cKO. No significant differences were observed in the percentage of bone volume over tissue volume, tissue surface area, or tissue surface perimeter in either sexes. Again, there seems to be a small difference between the sexes in that males seem to be slightly more affected by the Stat3 knockout in pre-osteoblasts than the females.

In the dynamic histomorphometry analyses, no significant differences were seen in the males, but several differences were observed in the females. In the trabecular region, cKO females had higher active osteoblast numbers as indicated by a higher MS/BS percentage. In the endocortical region, cKO females had significantly lower active osteoblast numbers, osteoblast activity, and bone formation rate as indicated by MS/BS, MAR, and BFR/BS, respectively. On the periosteal surface, cKO females actually had higher osteoblast activity and higher bone formation rate compared to WT controls. In females, there seems to be a substantial impairment of osteoblast function on the endocortical surface but not the periosteal surface. There is in fact an increase in function and bone formation rate on the periosteal surface of cKO females. The increase of activity on the periosteal surface could possibly exist in order to counteract the lack of activity on the endocortical surface. However, there is currently no other evidence of this provided by the current study.

Overall, there is a clear effect on skeletal development by Stat3 on osteoblasts. When Stat3 was conditionally knocked out in osteoblasts of developing mice, several different parameters were affected that led to a negative effect on bone development. Without Stat3, osteoblasts were unable to properly perform their jobs causing a decrease in size, femur length, and bone volume. This indicates that Stat3 is necessary for osteoblast differentiation and/or function. Because there is communication between osteoblasts and osteoclasts, the lack of Stat3 in osteoblasts could also have an indirect effect on osteoclasts. Osteoblasts are able to inhibit osteoclast activity through secretion of RANK decoy receptor OPG, so an impairment in osteoblast function by Stat3 could lead to a decrease in secretion of this receptor thus increasing osteoclast activity.

A study by Itoh et al. used a similar model that we used by incorporating an α1(I)-collagen Cre-LoxP to conditionally knock out Stat3 in osteoblasts. Mice lacking Stat3 in their osteoblasts had osteoporotic phenotypes, indicating their osteoblast function was impaired because of the lack of Stat3 (Itoh et al.). This was similar to our findings that osteoblasts need Stat3 in order for their osteoblasts to properly differentiate and function.

A study by Nicolaidou et al. also found similar results using an *in vitro* study where Stat3 was either overexpressed or knocked down in osteoblasts. They were able to demonstrate the necessity of Stat3 in differentiating osteoblasts from MSCs. While this study did not reveal any information on how function was affected, the study did confirm that Stat3 is important in osteoblast differentiation.

These studies did not provide any evidence of sex-based differences, but they did concur with our study that Stat3 is needed to differentiate osteoblasts and aid in their function. Our study did nonetheless highlight a probable sex-based difference which could be explored further in future studies.

4.2 Osteoclast *in vitro* Analysis

The microarray analysis paired with confirmatory results from the qPCR tests revealed a vast difference in gene expression between cells with normal levels of Stat3 in relation to the Stat3 knockdown cells when stimulated with RANKL for 24 hours. Several of the genes analyzed in the microarray and qPCR that significantly increased in response to Stat3 siRNA knockdown are known to be important – if not necessary – for osteoclastogenesis or osteoclast function such as Atp6v0d2, Cathepsin K, EEIG1 (aka FAM102A), and Src. This indicates that Stat3 is necessary for downregulating the transcriptional activity of factors needed in osteoclastogenesis. Because of this, Stat3 seems to have a negative effect on osteoclastogenesis, as well as osteoclast function.

In the western blot analyses, production of NFATc1 and Cathepsin K increased in response to Stat3 siRNA knockdown under RANKL stimulation. c-Fos production decreased slightly, though did not reach significance, in response to Stat3 siRNA knockdown. The upregulation or downregulation was partly dependent on the amount of time the cells were stimulated with RANKL. NFATc1 only appeared to be affected at 6 hours of stimulation with little effect at 24 hours.

When Stat3 was overexpressed, c-Fos increased somewhat but not significantly in samples with the Stat3 construct compared to samples with an empty plasmid. Based on the western blot for Stat3 knockdown in c-Fos, this result was expected. NFATc1

production exhibited no change at 6h between the RANKL control and overexpression groups. This is not the result that was expected based on the Stat3 knockdown western blots where NFATc1 increased when Stat3 was knocked down.

Taking all of the western blot experiments into account, Stat3 seems to have a somewhat positive role on c-Fos expression and production, a negative role on NFATc1 production, and a negative role in Cathepsin K production. Since c-Fos is known to upregulate NFATc1, this finding is curious. If Stat3 has no effect on, or even upregulates, c-Fos, seeing a similar effect on NFATc1 – and in turn, Cathepsin K – would be expected. However, this is not the case. Based on the negative effect Stat3 seems to have on NFATc1 and Cathepsin K, Stat3 appears to have a negative role in osteoclastogenesis and osteoclast function, as was also indicated by the microarray and qPCR analysis. The slight positive role Stat3 has on c-Fos is peculiar though and should be explored further.

TRAP staining revealed an increase in multi-nucleated osteoclast numbers when Stat3 was knocked down compared to the controls. This indicates that Stat3 could be suppressing osteoclast fusion and/or differentiation into multi-nucleated cells. The microarray and qPCR analyses revealed the inhibitory role Stat3 has on Atp6v0d2, which is important in osteoclast fusion. Therefore, the idea that Stat3 could be preventing fusion is entirely plausible. The microarray, qPCR, and western blot analyses all revealed several genes important for differentiation that Stat3 suppressed, such as NFATc1, so the TRAP stain could have simply revealed more evidence of the role Stat3 has in downregulating osteoclastogenesis.

Zhang et al. also studied the effect of Stat3 on osteoclasts *in vivo* and *in vitro* by conditionally knocking out Stat3 in hematopoietic stem cells (HSCs) of 3-4 week old mice using Tie2-Cre. When they conditionally knocked out Stat3 in osteoclasts, they believed there was an increase in osteoclast number that led to osteoporotic phenotypes (Z. Zhang et al.). Upon culturing these cells *in vitro* for further testing they found that c-Fos expression and production greatly increase in the absence of Stat3 (Z. Zhang et al.). Zhang et. al believed that Stat3 is a negative regulator of osteoclastogenesis due to its apparent inhibitory effect on c-Fos, which is needed for osteoclast differentiation (Z.

Zhang et al.). While our findings agree with this study in that Stat3 is a negative regulator of osteoclastogenesis, they disagree with this study in that we demonstrated that c-Fos levels increase when Stat3 levels increase, and c-Fos levels decrease when Stat3 is suppressed. While Stat3 has a negative role in many different important factors in osteoclastogenesis, it has an overall positive effect on c-Fos. Main differences in our studies are that we knocked down or overexpressed Stat3 while Zhang et. al conditionally knocked out Stat3. Additionally, this conditional knockout was not osteoclast-specific, rather it was for HSCs which differentiate into many different cell types. This could indicate that Stat3 acts as a switch for c-Fos that is stage-dependent. Before there is any commitment to the osteoclast lineage, Stat3 could be a negative regulator of c-Fos. Once cells have committed to the lineage, Stat3 could then act as a positive regulator of c-Fos.

Li et. al performed a study similar to ours by culturing murine osteoclast precursor RAW264.7 cells with M-CSF, RANKL, and varying concentrations of JAK inhibitor AG490. They found that the addition of AG490 inhibited osteoclast formation, leading them to believe that Stat3 must be a positive regulator of osteoclastogenesis (Li et al.). While this conclusion is relatively reasonable, one cannot definitively say whether Stat3 is a main factor in this regulation of osteoclastogenesis due to the wide array of cellular pathways JAK influences that do not directly involve Stat3. While these findings seem to contradict ours, the study we performed directly affected Stat3 while the study by Li et al. indirectly affected it. The effects they saw on osteoclastogenesis could be due to other factors affected by the JAK pathway that overpowered the effect on Stat3.

4.3 Future Directions

The osteoblast study revealed an overall positive effect of Stat3 on osteoblast differentiation. Osterix is important for osteoblast differentiation, and knocking Stat3 out at this stage had several major effects on bone development. Future studies could include knocking out Stat3 in different stages to elucidate its role on osteoblast function or other areas of osteoblast development more clearly. An *in vitro* study could also be useful in determining specifically what factors Stat3 is affecting within the cell that prevents proper differentiation. Further investigation could also be done on the potential sex

differences that occurred between the male and female mice. Males seemed to be more affected by the loss of Stat3 in pre-osteoblasts, so there could be factors in the female mice protecting them from equally damaging effect such as estrogen, which is thought to inhibit osteoclast differentiation (Kameda, Mano and Yuasa). Lower levels of bone resorption could help to offset the effect of less bone formation. Isolating osteoclasts from the WT and cKO mice to observe differences in function could be a useful next step to understand the potential sex difference seen in these mice. Another reason for this sex difference could be the relatively low number of animals used in the study. The cKO males were especially difficult to obtain, and only half the number of cKO males were available for the study compared to the other groups. In the future, a larger sample of animals should be obtained in order to increase the certainty of significance in these results.

The osteoclast study uncovered that Stat3 has more of a negative role in osteoclasts based on its effects on fusion, differentiation, and function. Because of this discovery, observing the role of Stat3 at each of these stages more carefully could be beneficial. The main factor observed in this study was differentiation, but observing the effect Stat3 has on osteoclast function could also be insightful. A useful experiment to find this information would be a bone resorption assay which could measure the activity of osteoclasts with normal levels of Stat3 and the activity of osteoclasts with higher or lower levels of Stat3 to see if osteoclast function is helped or hindered by a difference in Stat3 levels.

Another factor to examine in the osteoclast study is using further time points. This study observed the effect Stat3 has in earlier stages of osteoclastogenesis (3-24 hours), but further signaling events could be occurring later on. Samples could be collected at 48, 72, or even 96 hours to elucidate the role of Stat3 in later differentiation stages.

While this study revealed a negative effect Stat3 has on osteoclastogenesis, the pathways with which Stat3 exhibits this effect are still unclear. Further studies using qPCR and/or western blot analyses could be used on different genes known to be relevant for osteoclastogenesis to further explicate the pathways to which Stat3 affects

osteoclastogenesis. A good starting point might be TRAF6 since this is the earliest protein in the RANKL signaling cascade and is known to interact with Stat3 in other cells types (Wei, Yuan and Jin).

Along the same lines of looking more closely at the pathways Stat3 affects in osteoclastogenesis, a study could be done to find whether the proteins in this study are affected directly or indirectly by Stat3. It is already known that STAT proteins can bind the promoter region for c-Fos, causing a direct effect in its upregulation. It could be useful to find whether the same is true for NFATc1 and Cathepsin K or if Stat3 is causing an indirect effect by upregulating or downregulating other factors that induce these genes.

REFERENCES

Allen, Matthew R and David B Burr. "Bone Modeling and Remodeling." Allen, Matthew R and David B Burr. *Basic and Applied Bone Biology*. Amsterdam: Elsevier/Academic Press, 2014.

Andersen, Thomas Levin, et al. "A Physical Mechanism for Coupling Bone Resorption and Formation in Adult Human Bone." *The American Journal of Pathology* 174.1 (2009): 239-247. 31 May 2017.

Arboleya, Luis and Santos Castañeda. "Osteoimmunology: The Study of the Relationship Between the Immune System and Bone Tissue." *Reumatologia Clinica* 9.5 (2013): 303-315. 31 May 2017.

Bellido, Teresita, Lilian I. Plotkin and Angela Bruzzaniti. "Bone Cells." Burr, David B. and Matthew R. Allen. *Basic and Applied Bone Biology*. Amsterdam: Elsevier/Academic Press, 2014.

Bonewald, Lynda F. "The Amazing Osteocyte." *Journal of Bone and Mineral Research* 26.2 (2011): 229-238. 31 May 2017.

Bromberg, JF, et al. "Stat3 as an oncogene." *Cell* (1999): 295-303.

Buo, Atum M and Joseph P Stains. "Gap Junctional Regulation of Signal Transduction in Bone Cells." *FEBS Letters* 588.8 (2014): 1315-1321. 31 May 2017.

Burr, David B. and Akkus Ozan. "Bone Morphology and Organization." Burr, David B. and Matthew R. Allen. *Basic and Applied Bone Biology*. Amsterdam: Elsevier/Academic Press, 2014.

Carpenter, Richard L and Hui-Wen Lo. "STAT3 Target Genes Relevant to Human Cancers." *Cancers* (2014): 897-925. Document.

Carpenter, RL and HW Lo. "STAT3 Target Genes Relevant to Human Cancers." *Cancers (Basel)* 6.2 (2014): 897-925. 28 May 2017.

Clarke, Bart. "Normal Bone Anatomy and Physiology." *Clinical Journal of the American Society of Nephrology* 3.Suppl 3 (2008): S131–S139. 31 May 2017.

Cressman, Drew E, Robert H Diamond and Rebecca Taub. "Rapid activation of the stat3 transcription complex in liver regeneration." *Hepatology* 21.5 (1995): 1443-1449.

Dallas, Sarah L, Matthew Prideaux and Lynda F Bonewald. "The Osteocyte: An Endocrine Cell … and More." *Endocrine Reviews* 34.5 (2013): 658–690. 31 May 2017.

Dauer, Daniel J, et al. "Stat3 regulates genes common to both wound healing and cancer." *Oncogene* 24 (2005): 3397-3408. 28 May 2017.

Delgoffe, Greg M and Dario A A Vignali. "STAT Heterodimers in Immunity." *JAK-STAT* (2013): e23060. Document.

Engsig, Michael T, et al. "Matrix Metalloproteinase 9 and Vascular Endothelial Growth Factor Are Essential for Osteoclast Recruitment into Developing Long Bones." *The Journal of Cell Biology* 151.4 (2000): 879–890. 31 May 2017.

Fagard, Remi, et al. "STAT3 inhibitors for cancer therapy: Have all roads been explored?" *JAK-STAT* 2.1 (2013): e22882.

Fakhry, Maya, et al. "Molecular mechanisms of mesenchymal stem cell differentiation towards osteoblasts." *World Journal of Stem Cells* 5.4 (2013): 136-148. 31 May 2017.

Florencio-Silva, Rinaldo, et al. "Biology of Bone Tissue: Structure, Function, and Factors That Influence Bone Cells." *BioMed Research International* 2015 (2015): 421746. 31 May 2017.

Giacomelli, Mauro, et al. "SH2-domain mutations in STAT3 in hyper-IgE syndrome patients result in impairment of IL-10 function." *European Journal of Immunology* 41.10 (2011): 3075-3084. <http://dx.doi.org/10.1002/eji.201141721>.

Heinrich, Peter C, et al. "Principles of interleukin (IL)-6-type cytokine signalling and its regulation." *The Biochemical journal* 374.Pt 1 (2003): 1-20.

Holland, Steven M, et al. "STAT3 Mutations in the Hyper-IgE Syndrome." *The New England Journal of Medicine* 357 (2007): 1608-1619.

Itoh, Shousaku, et al. "A critical role for interleukin-6 family-mediated Stat3 activation in osteoblast differentiation and bone formation." *Bone* 39.3 (2006): 505-512. 30 May 2017.

Kameda, Takashi, et al. "Estrogen Inhibits Bone Resorption by Directly Inducing Apoptosis of the Bone-resorbing Osteoclasts." *The Journal of Experimental Medicine* (1997): 489-495. Document.

Kapinas, Kristina, et al. "miR-29 Modulates Wnt Signaling in Human Osteoblasts through a Positive Feedback Loop." *Journal of Biological Chemistry* 285.33 (2010): 25221–25231. 31 May 2017.

Khosla, Sundeep, Merry Jo Oursler and David G Monroe. "Estrogen and the Skeleton." *Trends in Endocrinology and Metabolism* 23.11 (2012): 576-581. 31 May 2017.

Li, C, et al. "AG490 inhibits NFATc1 expression and STAT3 activation during RANKL induced osteoclastogenesis." *Biochemical and Biophysical Research Communications* 435.4 (2013): 533-539.

Lodish, Harvey, et al. *Molecular Cell Biology*. New York: W. H. Freeman and Company, 2008.

Mantel, C, et al. "Mouse hematopoietic cell-targeted STAT3 deletion: stem/progenitor cell defects, mitochondrial dysfunction, ROS overproduction, and a rapid aging-like phenotype." 120.13 (2015).

Minegishi, Yoshiyuki and Hajime Karasuyama. "Genetic origins of hyper-IgE syndrome." *Current allergy and asthma reports* 8.5 (2008): 386-391.

Mogensen, Trine H. "STAT3 and the Hyper-IgE syndrome: Clinical presentation, genetic origin, pathogenesis, novel findings and remaining uncertainties." *JAK-STAT* 2.2 (2013): e23435.

Nicolaidou, Vicky, et al. "Monocytes Induce STAT3 Activation in Human Mesenchymal Stem Cells to Promote Osteoblast Formation." *PLoS One* 7.7 (2012): e39871. 29 May 2017.

Okamoto, Kazuo and Hiroshi Takayanagi. "Regulation of bone by the adaptive immune system in arthritis." *Arthritis Research and Therapy* 13.3 (2011): 219.

Park, Keun Woo, et al. "Mitochondrial STAT3 is negatively regulated by SOCS3 and upregulated after spinal cord injury." 284 (2016).

Rebe, Cedric, et al. "STAT3 Activation: A key factor in tumor immunoescape." *JAK-STAT* 2.1 (2013). 28 May 2017.

Solomon, Eldra P., Linda R. Berg and Diana W. Martin. *Biology*. Belmont: Brooks Cole, 2007.

Sowerwine, KJ, et al. "Bone density and fractures in autosomal dominant hyper IgE syndrome." *Journal of Clinical Immunology* 34.2 (2014): 260-264.

Teitelbaum, Steven L. "Osteoclasts: What Do They Do and How Do They Do It?" *The American Journal of Pathology* 170.2 (2007): 427-435. 31 May 2017.

Timofeeva, OA, et al. "Mechanisms of unphosphorylated STAT3 transcription factor binding to DNA." *The Journal of biological chemistry* 287.17 (2012): 14192-14200.

Wei, Juncheng, et al. "The Ubiquitin Ligase TRAF6 Negatively Regulates the JAK-StAT Signaling Pathway by Binding to STAT3 and Mediating Its Ubiquitination." 7.11 (2012).

Xu, L, et al. "The STAT3 HIES mutation is a gain-of-function mutation that activates genes via AGG-element carrying promoters." *Nucleic acids research* 43.18 (2015): 8898-8912.

Yu, Hua, et al. "Revisiting STAT3 signalling in cancer: new and unexpected biological functions." *Nature Reviews Cancer* 14.11 (2014): 736-746.

Zhang, Huiyuan, et al. "STAT3 restrains RANK- and TLR4-mediated signaling by suppressing expression of the E2 ubiquitin ligase Ubc13." 5.5798 (2015).

Zhang, Ying, et al. "A program of microRNAs controls osteogenic lineage progression by targeting transcription factor Runx2." *Proceedings of the National Academy of Sciences of the United States of America* 108.24 (2011): 9863–9868. 31 May 2017.

Zhang, Z, et al. "Osteoporosis with increased osteoclastogenesis in hematopoietic cell-specific STAT3-deficient mice." *Biochemical and Biophysical Research Communications* 328.3 (2005): 800-807.

Zhou, Hongkang, et al. "Osteoblast/osteocyte-specific inactivation of Stat3 decreases load-driven bone formation and accumulates reactive oxygen species." 49.3 (2011).

TABLES

Table 1: Comprehensive qPCR primer list

Gene	Forward Primer	Reverse Primer
Slc6a4 (5-HTT)	5′-GACCAGTGTGGTGAACTGCATGAC-3′	5′-GATGATGGCAAAGAATGTGGATGCTG-3′
Nhedc2	5'-GCAGCTGGATCTTTTCTTGG-3'	5'-TCTTCCAGCTGCTTCTCTCC-3'
Serpinb6b	5'-GCCAATATAGGTTTTAGGTGATATGGTCC-3'	5'-GCTATGCAGTTGAGGCTAGCCCTGCATG-3'
Pdgfb	5′-CGCGGATCCACCATGAATCGCTGCTGG-3′	5′-CCGCTCGAGCTAGGCTCCAAGGGTCTC-3′
Src	5′-CCAGGCTGAGGAGTGGTACT-3′	5′-CAGCTTGCGGATCTTGTAGT-3′
Atp6v0d2	5′-GACCCTGTGGCACTTTTTGT-3′	5′-GTGTTTGAGCTTGGGGAGAA-3′
Fam102a	5′-CTCAGTATGGCTGTAGAGGG-3′	5′-ATCTTCTCCACAATGTCGTC-3′
Edil3 (DEL1)	5′-ATATAGTGCGCTCCTGGCCTCA-3′	5′-AGCCTATGAATGTGTCTCCTCGA-3′
Cybb (NOX-2)	5′-ACCGCCATCCACACAATTG-3′	5′-CCGATGTCAGAGAGAGCTATTGAA -3′
Cebpa	5'-ATAAAGCCAAACAGCGCAAC-3'	5'-CGGTCATTGTCACTGGTCAA-3'
Icam2	5'-ACCTGTAACCAGCCTGAAGT-3'	5'-TTGGAGGCTGGTACACGCTG-3'
Sla	5′-AGATTGGTAGCTTCATGATTCG-3′	5′-GGTGAGTCTCACCTGCTTAG-3′
Rorc	5′-CCGAGGATGAGATTGCCCTCT-3′	5′-GGTGGCAGCTTTGCCAGGAT-3′
Ifi202b	5'-GGCAATGTCCAACCGTAACT-3'	5'-TAGGTCCAGGAGAGGCTTGA-3'
Hyal1	5′-CCTTCAGTCCTGAGGTTTCCC-3′	5′-CTCCATACTCCGTCAGGCAC-3′
Hyal1	5′-CCCTTCAGTCCTGAGGTTTCC-3′	5′-CACTCCATACTCCGTCAGGC-3′
Dmpk	5′-CTTCTACGCGGACTCCACAG-3′	5′-CTCGAAGTCTGCCCCACCTC-3′
Bcar3	5′-ACCAGCCTCTTGGCGGA -3′	5′-CATGATTCTTAACTCTCCCCGC-3′
Hoxa1	5′-CAGGAAGCAGACCCACCAAG-3′	5′-CCACGTAGCCGTACTCTCCA-3′
Hoxa1	5′-CAGGAAGCAGACCCACCAAG-3′	5′-ACCCACGTAGCCGTACTCTC-3′
Ptgs1 (COX-1)	5′-CCTCAGGGCAGATATCCTAGAGTTC-3′	5′-GCAGTCCAGGTTCCAATTGTC-3′
Gadd45g	5′-GGATAACTTGCTGTTCGTGGA-3′	5′-AAGTTCGTGCAGTGCTTTCC-3′
Cd97	5′-CCCGGCACTTTCCTGTTACT-3′	5′-AAATGCACACCACAAGCAGG-3′
Cd97	5′-CTGCATAAAAGCCCAGCCCA-3′	5′-GCACAGTTCTTACTCTCTGCCT-3′
S1pr1	5′-AGCTCAGGGAACTTTGCGAG-3′	5′-GAGAAACAGCAGCCTCGCTC-3′
S1pr1	5′-TCAGGGAACTTTGCGAGTGAG-3′	5′-TCCGAGAAACAGCAGCCTCG-3′
Nfkbie	5′-GGCTGAGGACCTCCTTTCTT-3′	5′-CCATCCGAGCTTCAGTCAGTA-3′
Nfkbie	5′-GGCTGAGGACCTCCTTTCTTAT-3′	5′-CCGAGCTTCAGTCAGTACAT-3′
AMPK (Prkaa1)	5′-GGGTGAAGATCGGCCACTAC-3′	5′-TGCTTGCCCACCTTCACTTT-3′
AMPK (Prkaa1)	5′-CGCAGACTCAGTTCCTGGAG-3′	5′-GCTTGCCCACCTTCACTTTC-3′
UCP2	5′-TGTGCCCTTACCATGCTCCA-3′	5′-AGGGCTCGTTTCAGCTGCTC-3′
PPARγ	5′-TGTGGGGATAAAGCATCAGGC-3′	5′-CCGGCAGTTAAGATCACACCTAT-3′
Mapk11	5′-GGCTGATGAGGAGATGACCG-3′	5′-CAGCTGGTCGATGTAGTCGT-3′
Mapk11	5′-ACCTGAAGCACGAGAACGTC-3′	5′-TGGATATACTTCAGCCCACGC-3′
Oscar	5′-TGATTGGCACAGCAGGAG-3′	5′-AAGGCACAGGAAGGAAATAGAG-3′
GLUT1	5'-ACTGGGCAAGTCCTTTGAGAT-3'	5'-GTCCTTGTTGCCCATGATGGA-3'
Mitf	5′-GGGATTGATGGATCCTGCTTTG-3′	5′-GGCTGGACAGGAGTTGCTGA-3′
PU.1	5′-TACCAACGTCCAATGCATGA-3′	5′-GCTGGGGACAAGGTTTGATA-3′
Akt	5′-TGTCTGCCCTGGACTACTTGC-3′	5′-GGCGTTCCGCAGAATGTC-3′
DC-STAMP	5′-TCCTCCATGAACAAACAGTTCCAA-3′	5′-AGACGTGGTTTAGGAATGCAGCTC-3′

Table 2: KEGG pathway analysis based on microarray data

Pathway	**Ratio**	***p***
Rheumatoid arthritis	10.44	3.42e-06
Lysosome	6.18	0.0007
Regulation of actin cytoskeleton	3.97	0.0055
Collecting duct acid secretion	12.52	0.0062
Amoebiasis	5.15	0.0066
Phagosome	3.98	0.0138
Cell adhesion molecules (CAMs)	4.08	0.0202

FIGURES

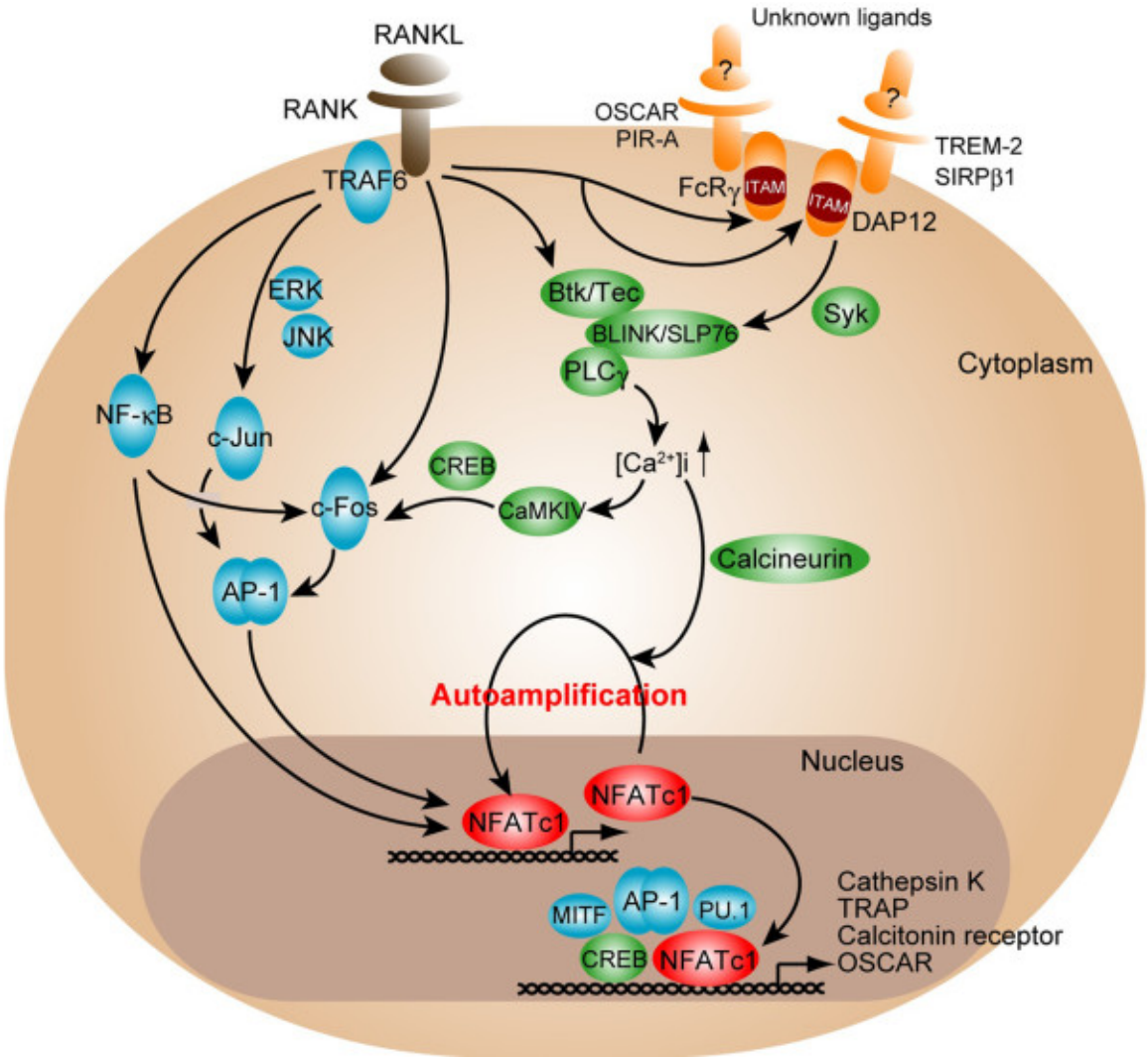

Figure 1: Intracellular pathway of osteoclast being induced by RANKL (Okamoto and Takayanagi)

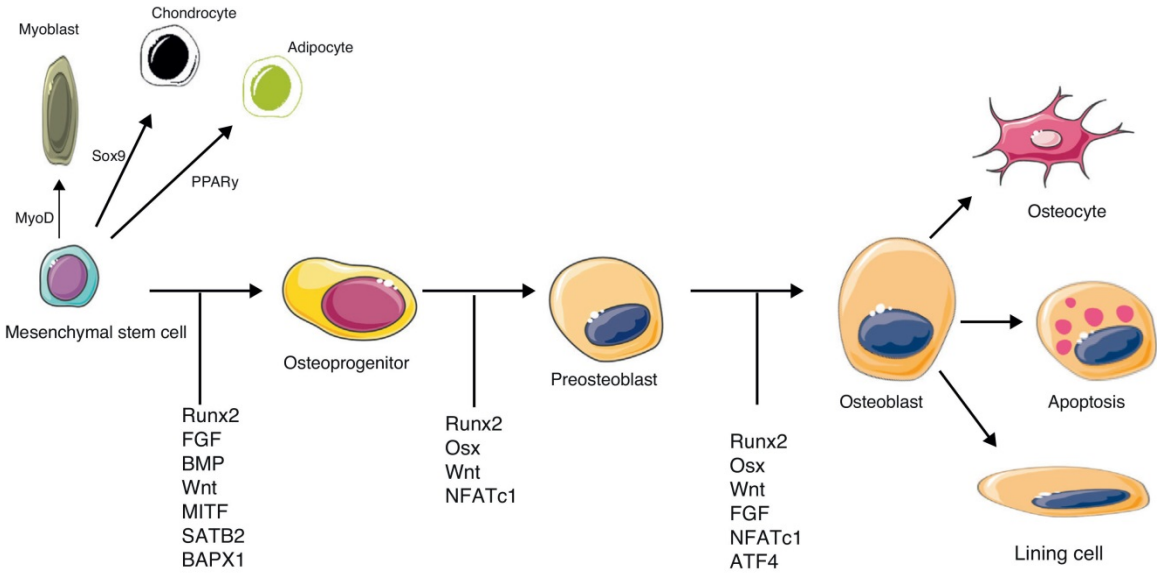

Figure 2: Osteoblast differentiation pathway (Arboleya and Castañeda)

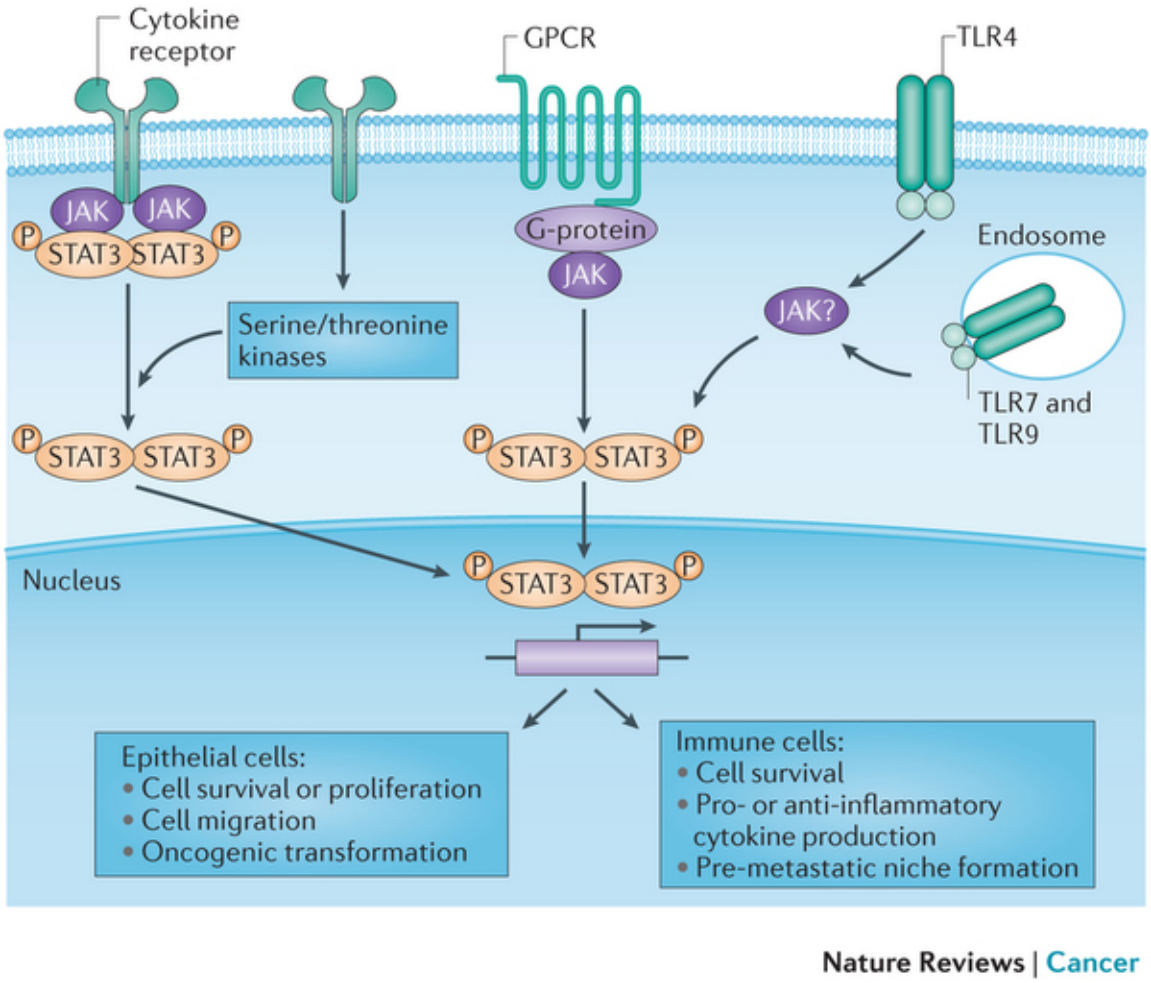

Figure 3: Stat3 signaling pathways (Yu et al.)

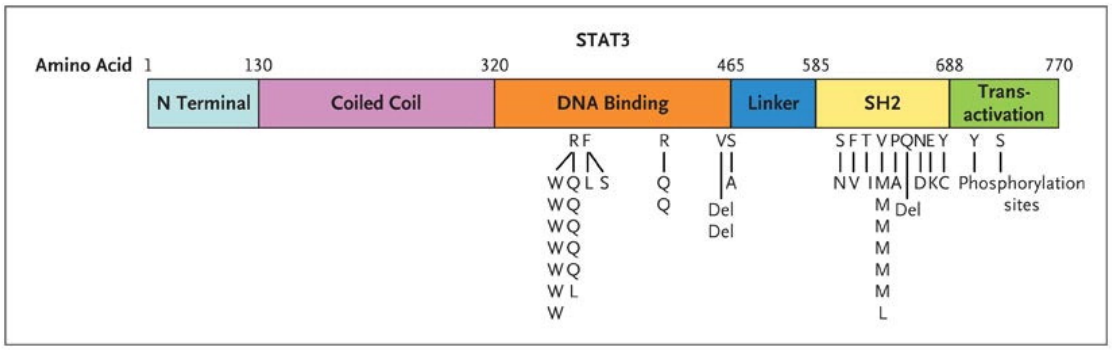

Figure 4: Stat3 structure with listed mutations (Holland et al.)

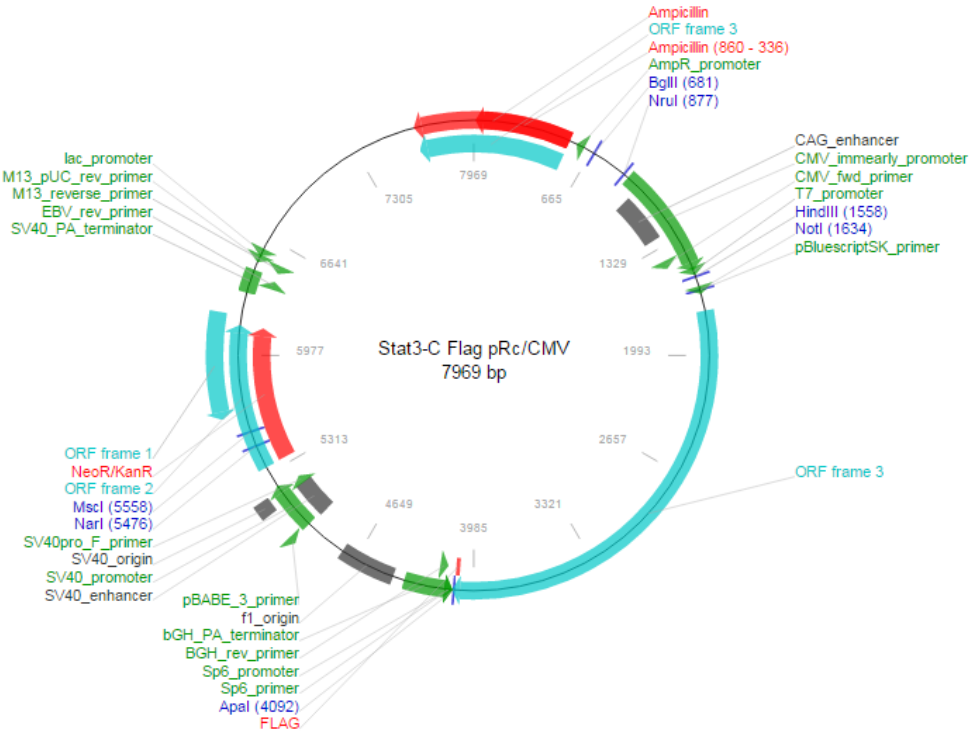

Figure 5: Stat3-C Flag pRc/CMV 7969 bp overexpression construct (Bromberg et al.).

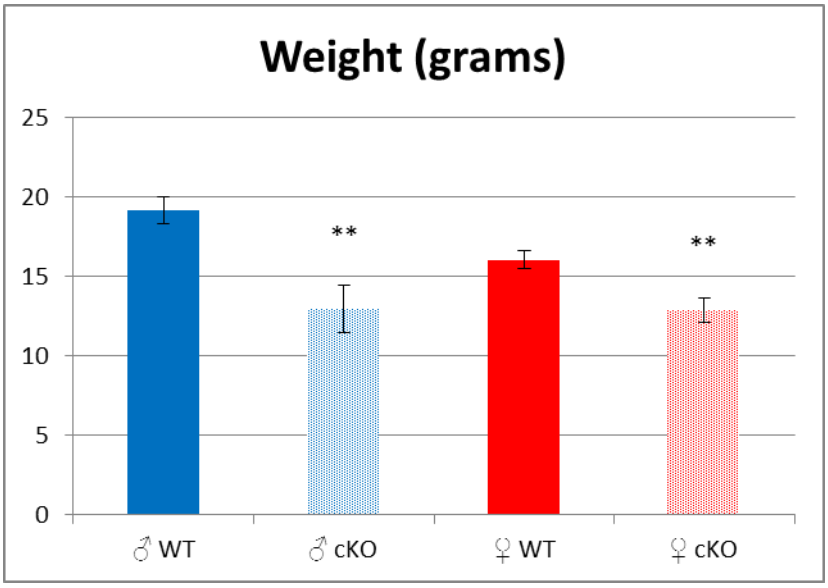

Figure 6: Body weights of experimental mice at 8 weeks of age. Highly significant decrease in weight observed between WT males and cKO males as well as WT females and cKO females.

Figure 7: Female WT (left) and female cKO (right) at 7 weeks

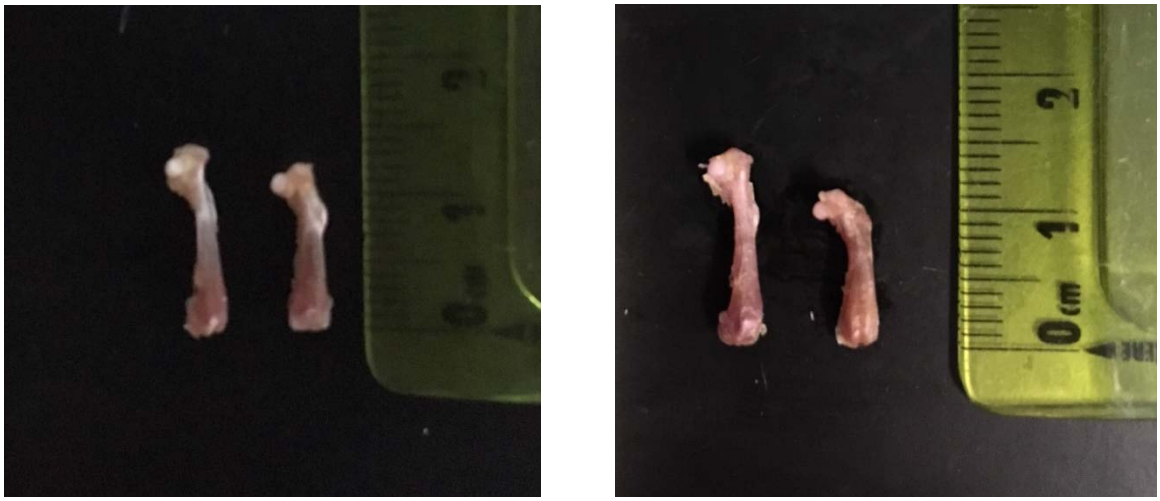

Figure 8: Dissected femurs of male (left) and female (right) 8-week mice. In both images, the femur to the left is WT and the femur to the right is cKO. Both sexes exhibited a highly significant decrease in length in cKO in comparison to their WT counterparts.

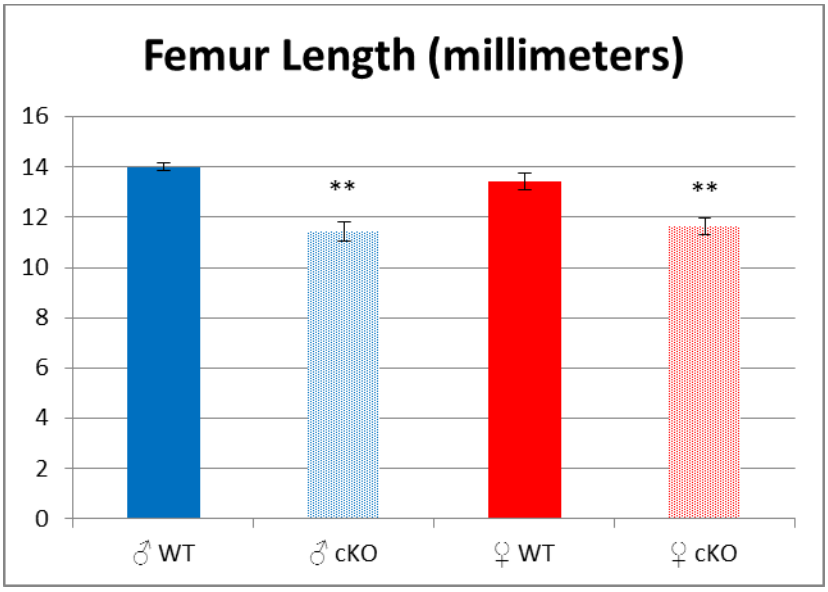

Figure 9: Femur lengths of experimental mice at 8 weeks of age. Highly significant decrease in femur length observed between WT males and cKO males as well as WT females and cKO females.

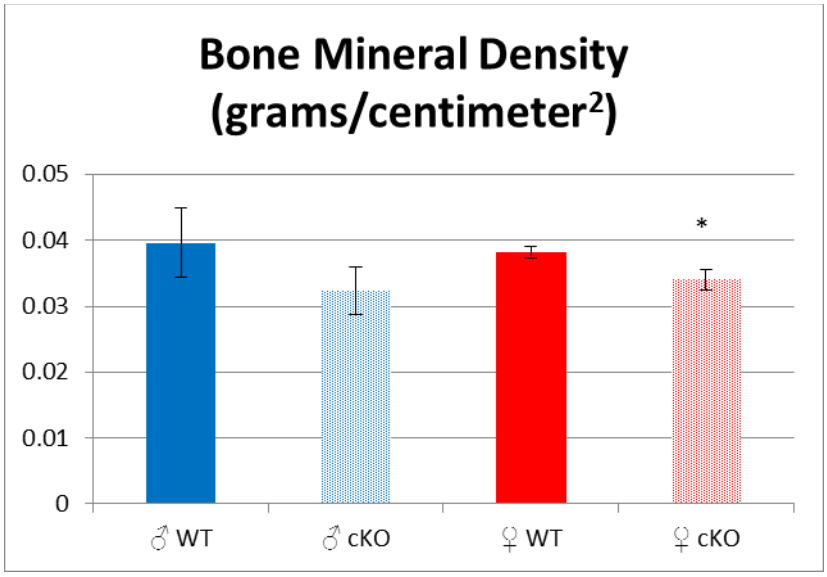

Figure 10: Bone mineral density of experimental mice at 8 weeks of age. No significant difference between WT males and cKO males. Significant decrease in BMD observed between WT females and cKO females.

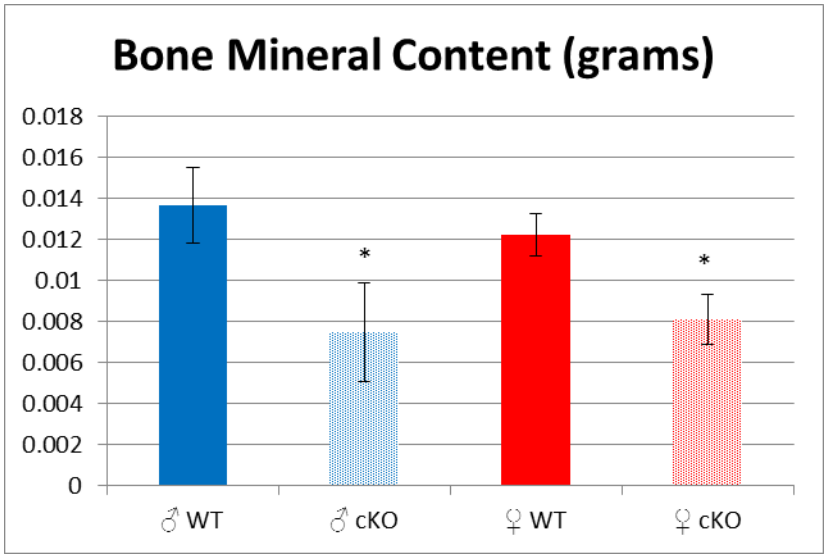

Figure 11: Bone mineral content of experimental mice at 8 weeks of age. Significant decrease observed between WT males and cKO males as well as WT females and cKO females.

Figure 12: Micro CT analysis of 8-week mouse femurs. From left to right: WT males (A), cKO males (B), WT females (C), and cKO females (D). cKO mice of both sexes had shorter femurs that had a metaphyseal defect indicated by the arrow.

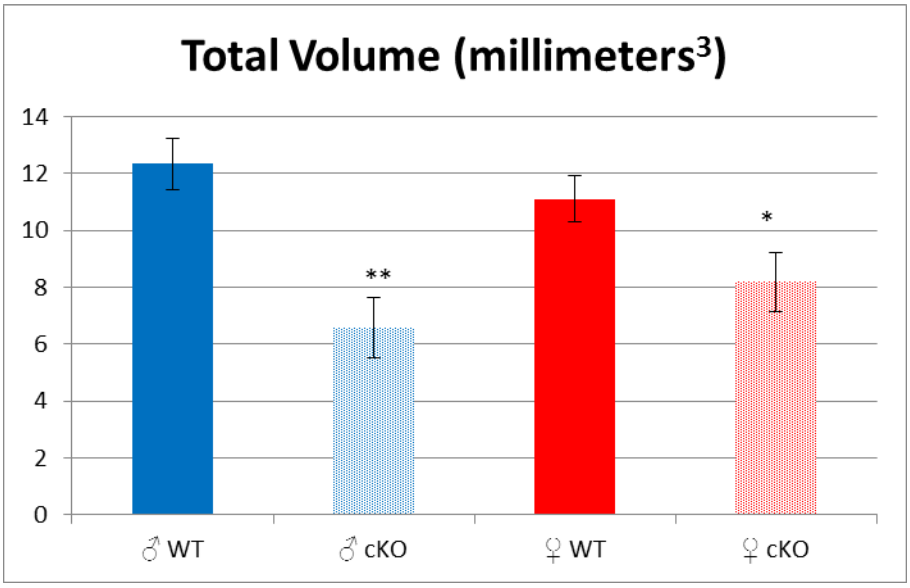

Figure 13: Total volume of cortical region based on Micro-CT analysis in experimental mice at 8 weeks of age. Highly significant decrease observed between male WT and cKO mice. Significant decrease observed between female WT and cKO mice.

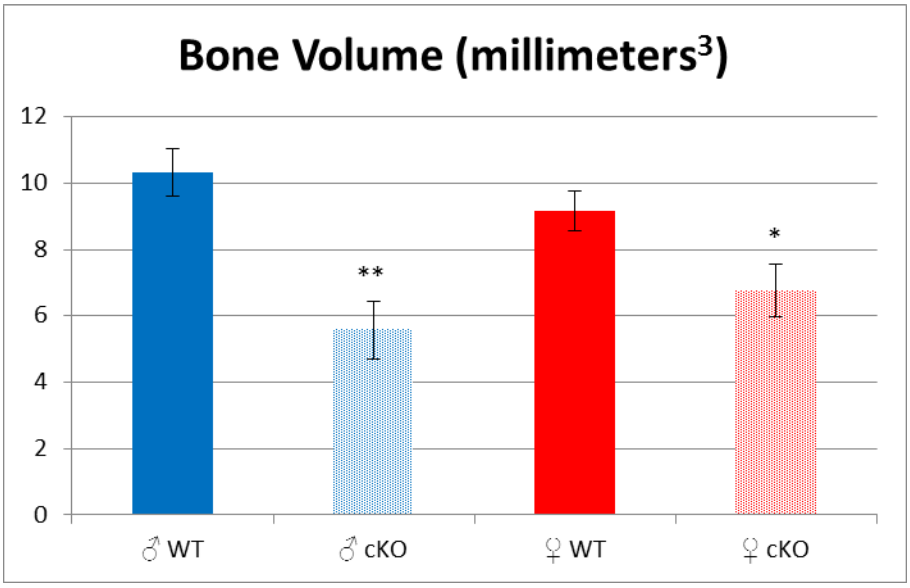

Figure 14: Bone volume of cortical region based on Micro-CT analysis in experimental mice at 8 weeks of age. Highly significant decrease observed between male WT and cKO mice. Significant decrease observed between female WT and cKO mice.

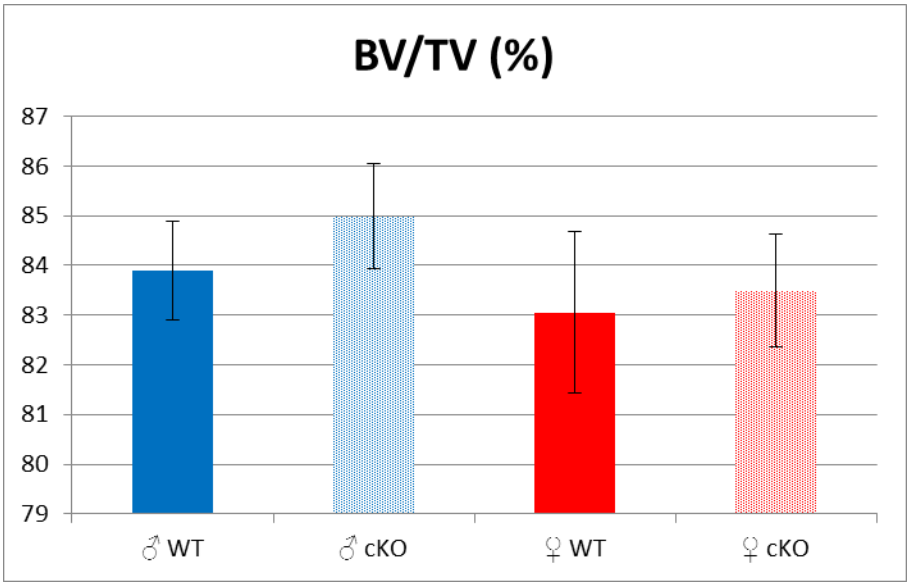

Figure 15: Bone volume over tissue volume of cortical region based on Micro-CT analysis in experimental mice at 8 weeks of age. No significant changes were seen between WT or cKO in either the males or the females.

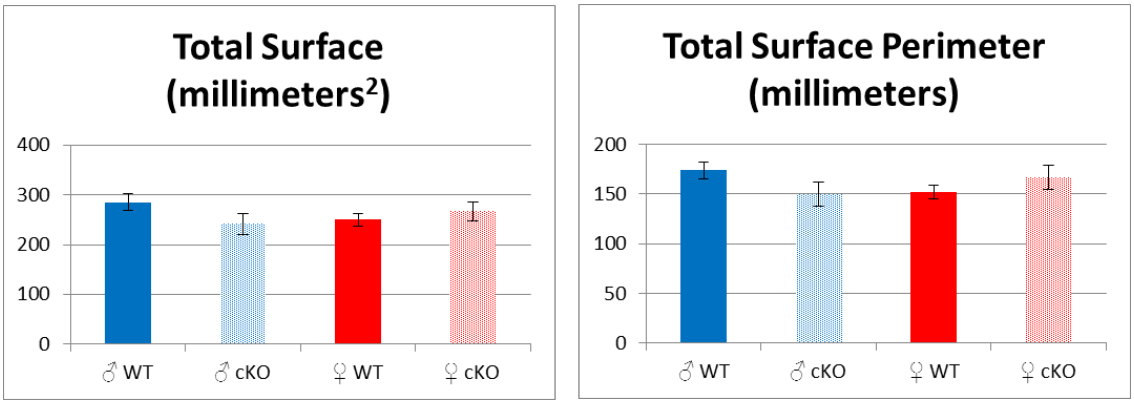

Figure 16: Total surface area and perimeter of cortical region based on Micro-CT analysis in experimental mice at 8 weeks of age. No significant changes were seen between WT or cKO in either the males or the females.

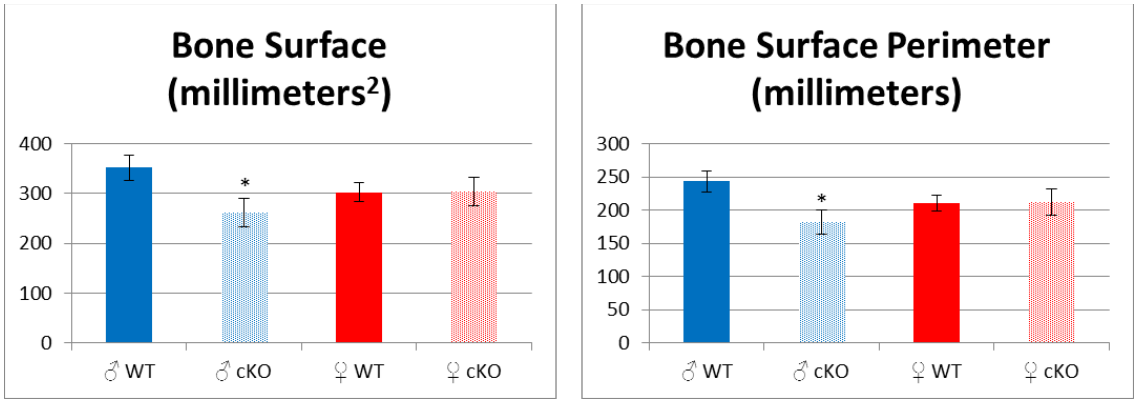

Figure 17: Bone surface area and perimeter of cortical region based on Micro-CT analysis in experimental mice at 8 weeks of age. A significant decrease was seen from the WT to the cKO males in both categories. No significant change was seen in females.

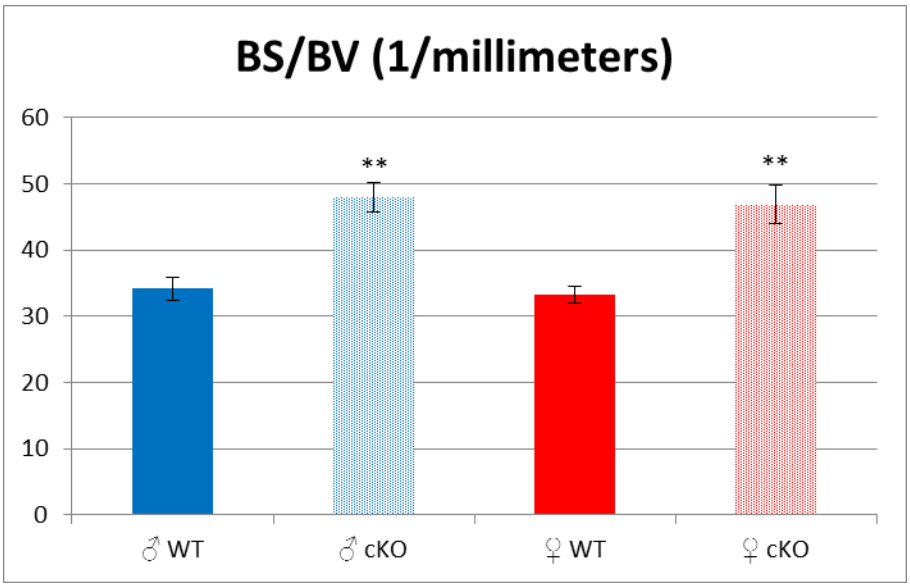

Figure 18: Bone surface over bone volume of cortical region based on Micro-CT analysis in experimental mice at 8 weeks of age. A highly significant increase was seen from the WT to the cKO in both males and females.

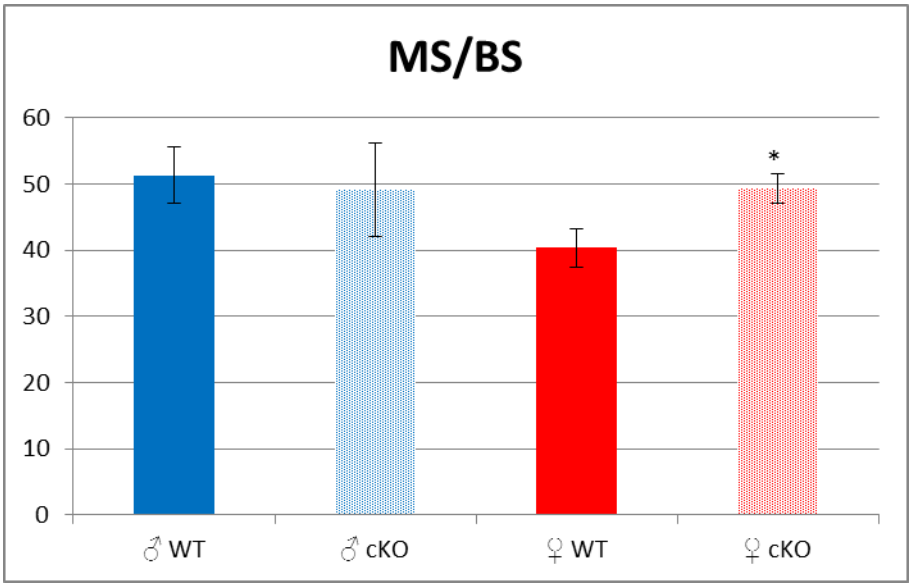

Figure 19: Dynamic histomorphometry of trabecular region showing mineralizing surface over bone surface. A significant increase was seen in cKO females compared to WT females. No significant difference was seen in males.

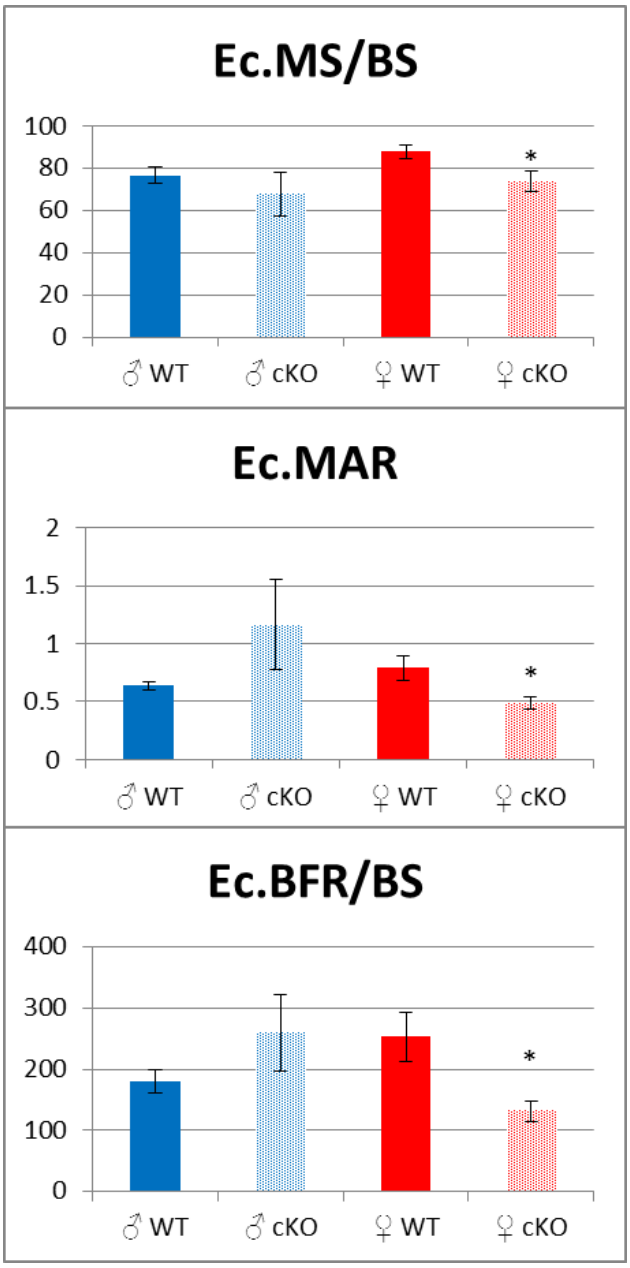

Figure 20: Endocortical surface parameters showing significant decrease in cKO females for mineralizing surface over bone surface, mineral apposition rate, and bone formation rate over bone surface. No significant difference was seen in males.

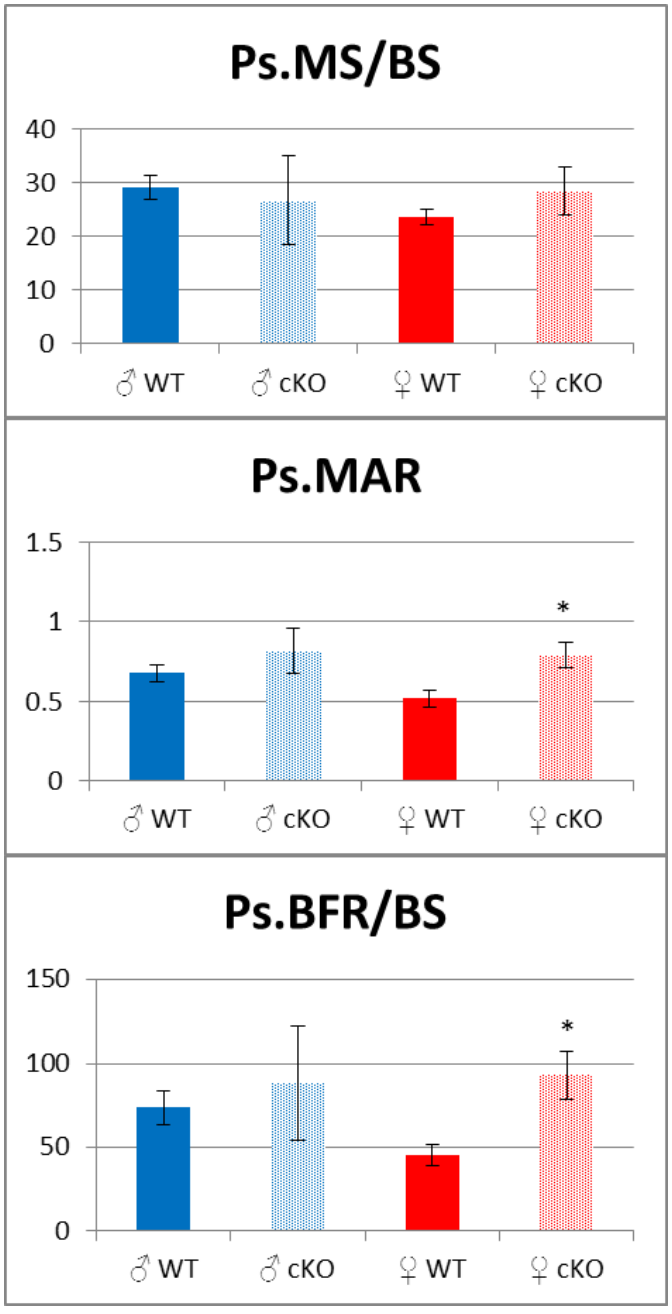

Figure 21: Periosteal surface parameters showing significant increase in cKO females for mineral apposition rate and bone formation rate over bone surface. No significant difference was seen for either sexes in mineralizing surface over bone surface. No significant change was seen in males.

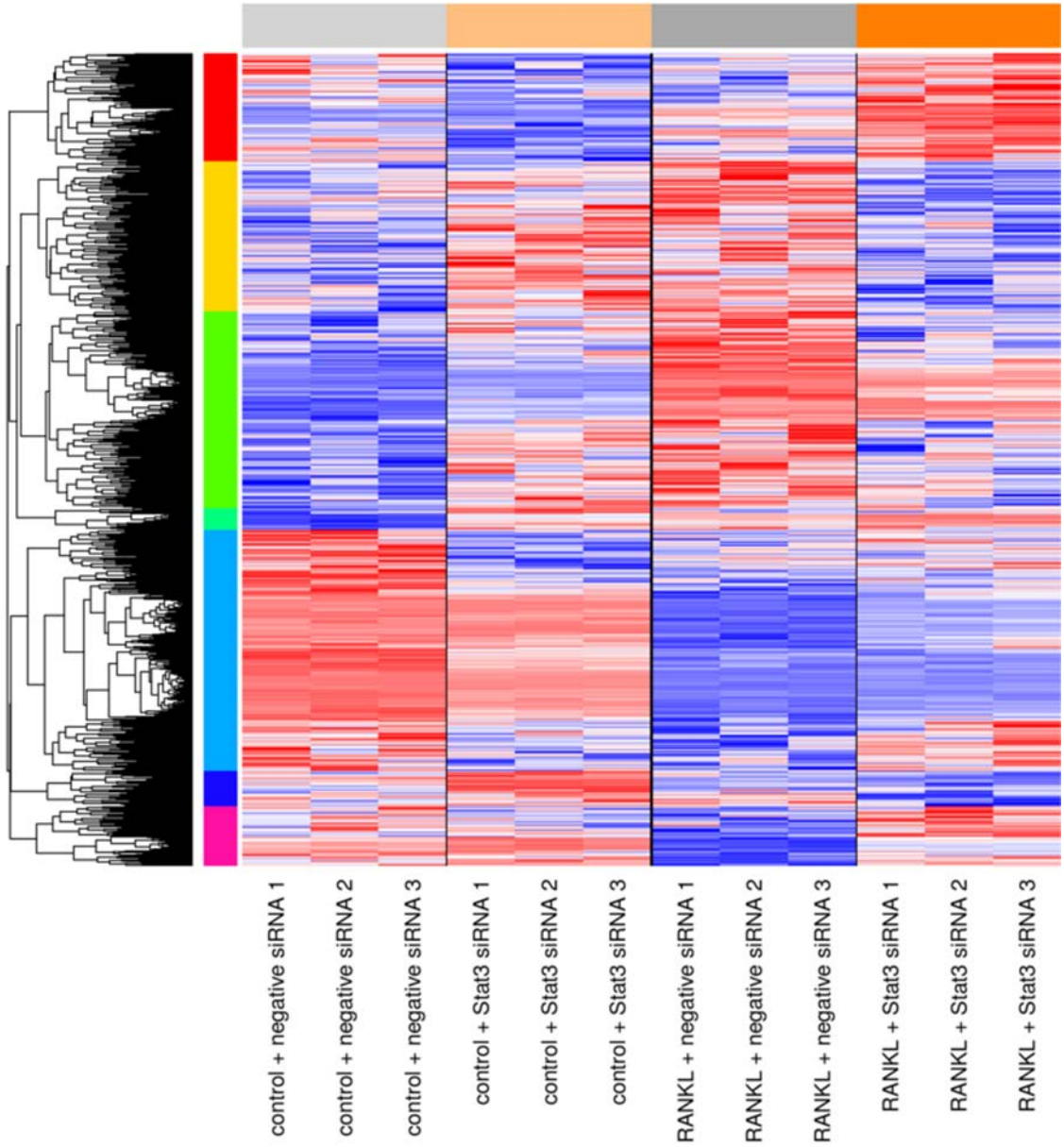

Figure 22: Microarray heat map of 24 hour RANKL samples.

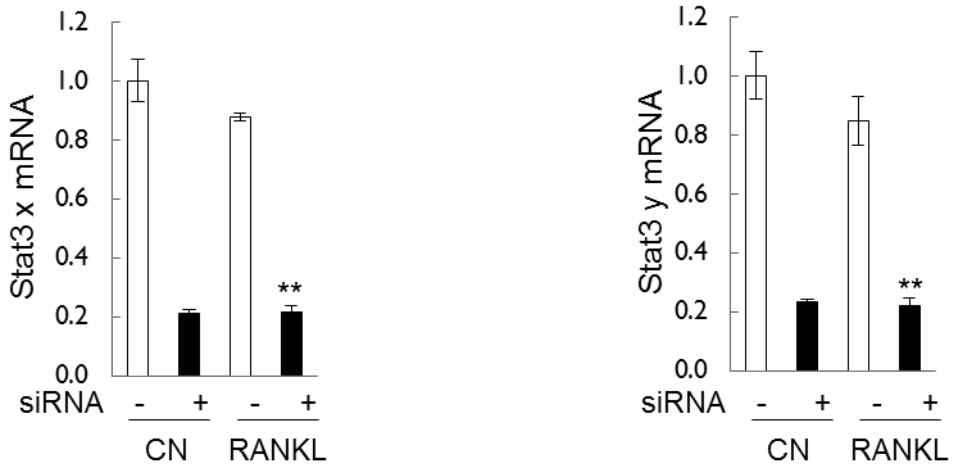

Figure 23: qPCR analysis of Stat3 primer showing highly significant knockdown compared to non-specific controls.

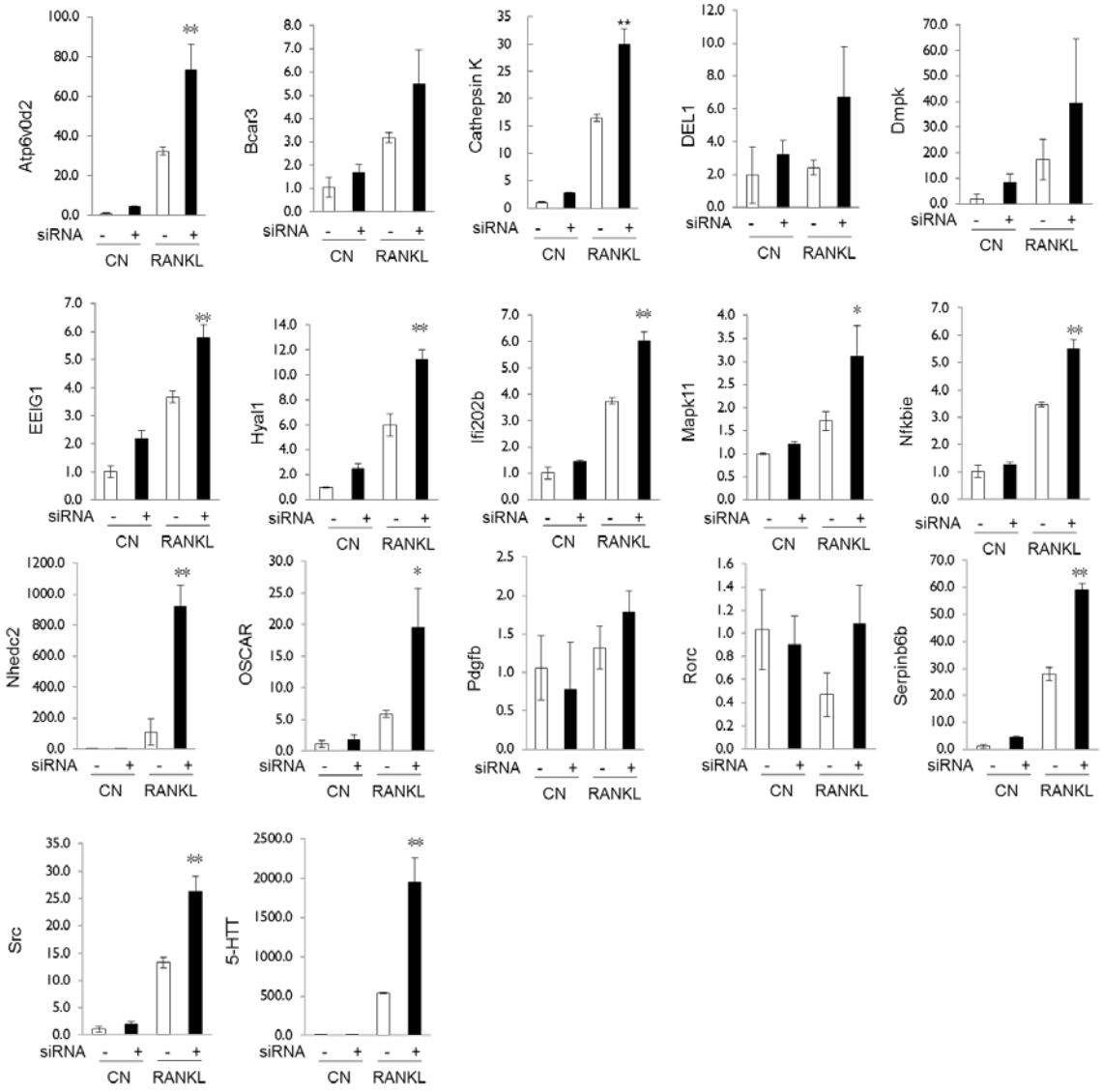

Figure 24: qPCR analysis of genes upregulated in Stat3 siRNA 24 hour RANKL groups.

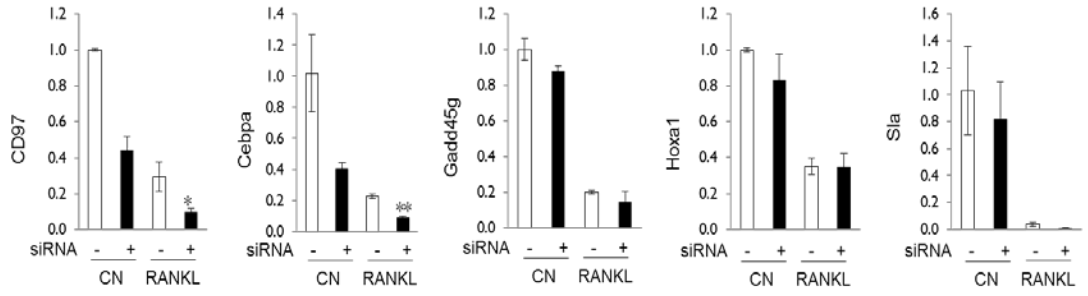

Figure 25: qPCR analysis of genes downregulated in Stat3 siRNA 24 hour RANKL groups.

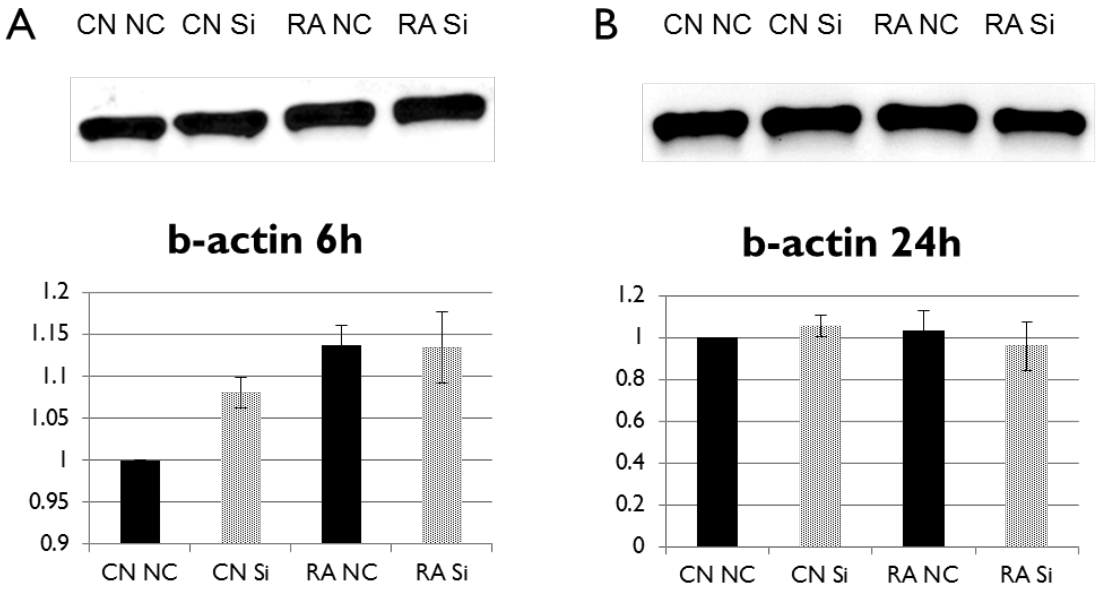

Figure 26: Western blot b-actin bands of Stat3 siRNA knockdown samples quantified with relative density at 6 hours (A) and 24 hours (B). Each band from left to right represents pre-osteoclast control, pre-osteoclast with Stat3 siRNA, RANKL-stimulated osteoclast control, and RANKL-stimulated with Stat3 siRNA.

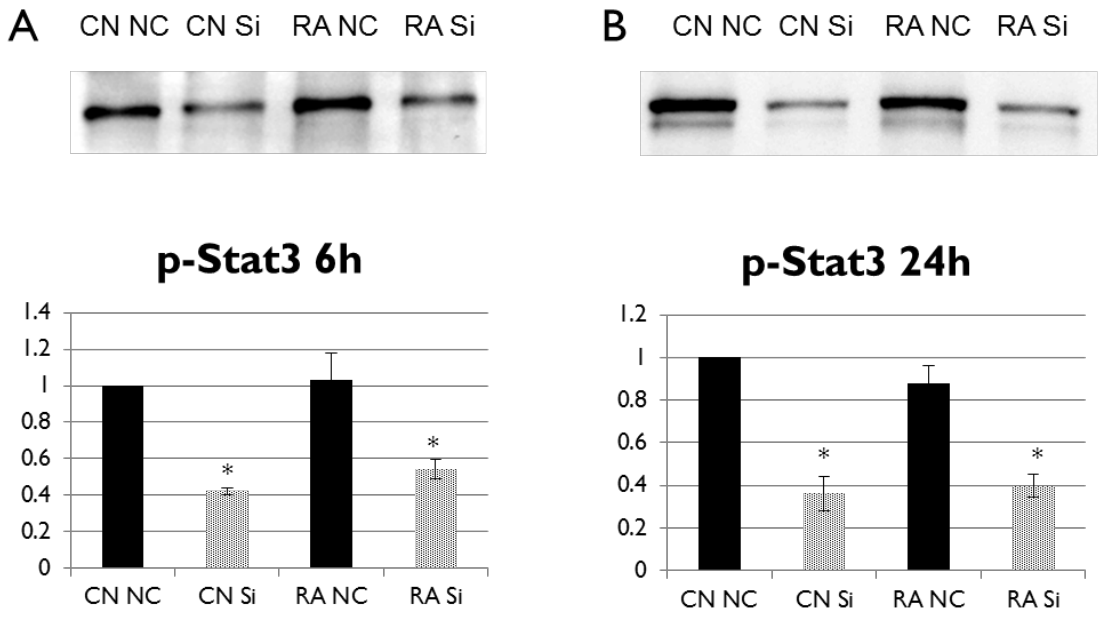

Figure 27: Western blot p-Stat3 bands of Stat3 siRNA knockdown samples quantified with adjusted density to b-actin at 6 hours (A) and 24 hours (B). Each band from left to right represents pre-osteoclast control, pre-osteoclast with Stat3 siRNA, RANKL-stimulated osteoclast control, and RANKL-stimulated with Stat3 siRNA.

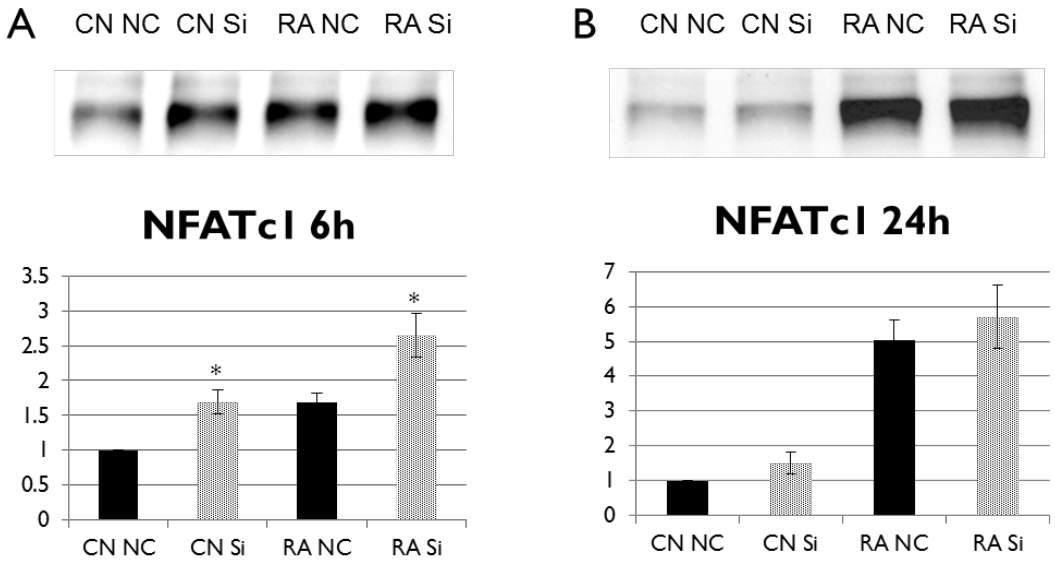

Figure 28: Western blot NFATc1 bands of Stat3 siRNA knockdown samples quantified with adjusted density to b-actin at 6 hours (A) and 24 hours (B). Each band from left to right represents pre-osteoclast control, pre-osteoclast with Stat3 siRNA, RANKL-stimulated osteoclast control, and RANKL-stimulated with Stat3 siRNA.

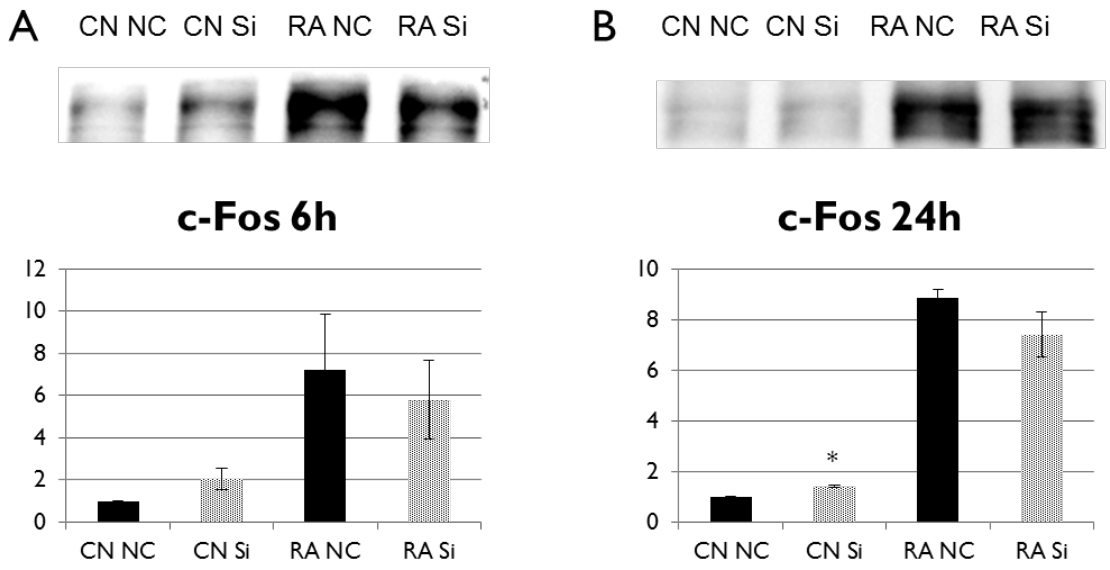

Figure 29: Western blot c-Fos bands of Stat3 siRNA knockdown samples quantified with adjusted density to b-actin at 6 hours (A) and 24 hours (B). Each band from left to right represents pre-osteoclast control, pre-osteoclast with Stat3 siRNA, RANKL-stimulated osteoclast control, and RANKL-stimulated with Stat3 siRNA.

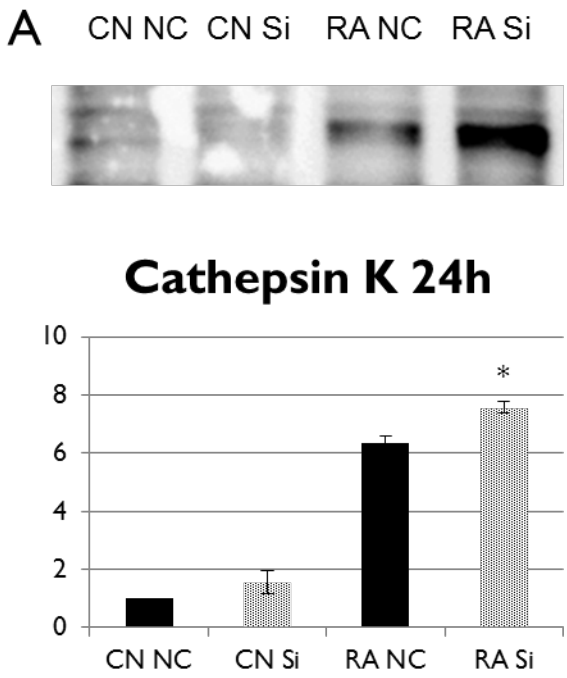

Figure 30: Western blot Cathepsin K bands of Stat3 siRNA knockdown samples quantified with adjusted density to b-actin at 24 hours (A). Each band from left to right represents pre-osteoclast control, pre-osteoclast with Stat3 siRNA, RANKL-stimulated osteoclast control, and RANKL-stimulated with Stat3 siRNA.

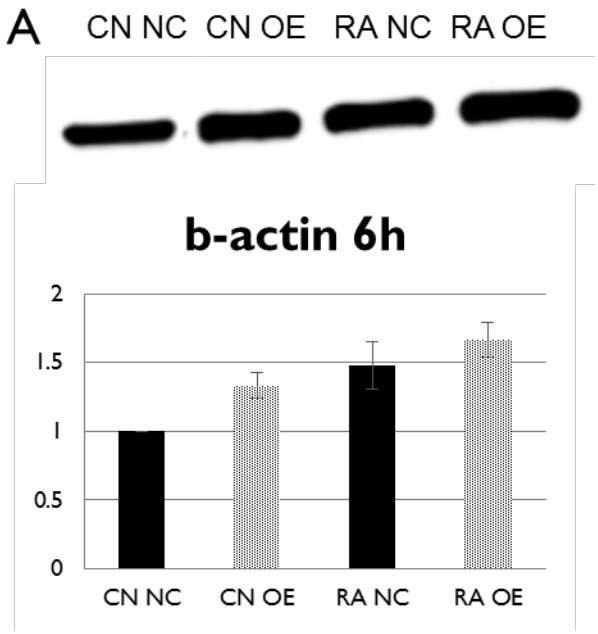

Figure 31: Western blot b-actin bands of Stat3 overexpression construct samples quantified with relative density at 6 hours (A). Each band from left to right represents pre-osteoclast control, pre-osteoclast with Stat3 construct, RANKL-stimulated osteoclast control, and RANKL-stimulated with Stat3 construct.

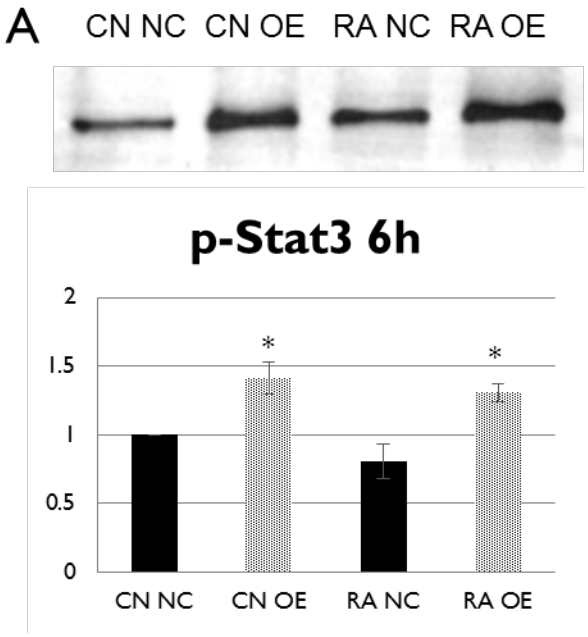

Figure 32: Western blot p-Stat3 bands of Stat3 overexpression construct samples quantified with relative density at 6 hours (A). This graph illustrates the significant increase in Stat3 production for both overexpression groups.

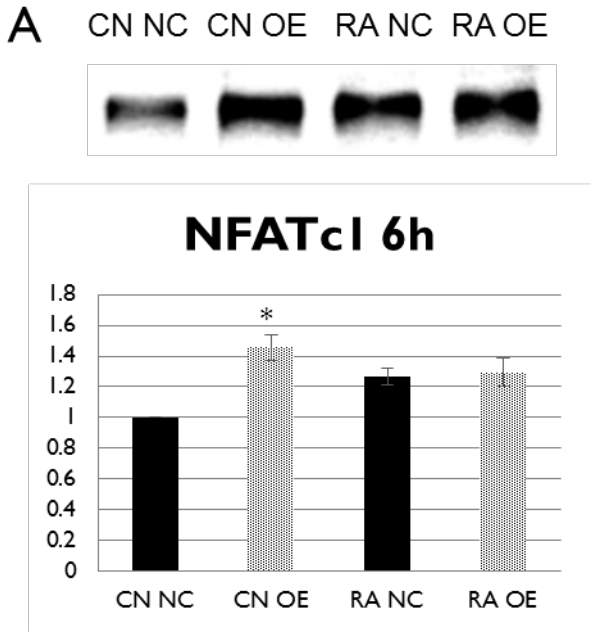

Figure 33: Western blot NFATc1 bands of Stat3 overexpression construct samples quantified with relative density at 6 hours (A). This graph illustrates there is no significant difference between the RANKL groups when Stat3 is overexpressed.

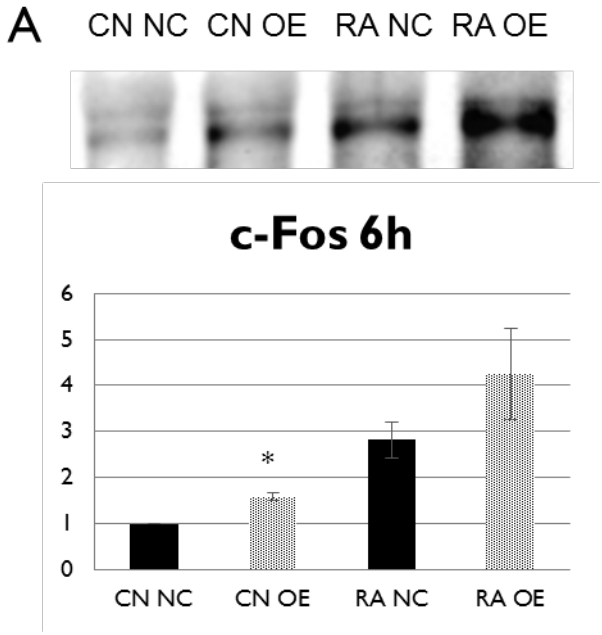

Figure 34: Western blot c-Fos bands of Stat3 overexpression construct samples quantified with relative density at 6 hours (A). This graph demonstrates a slight but insignificant increase in c-Fos production when Stat3 is overexpressed.

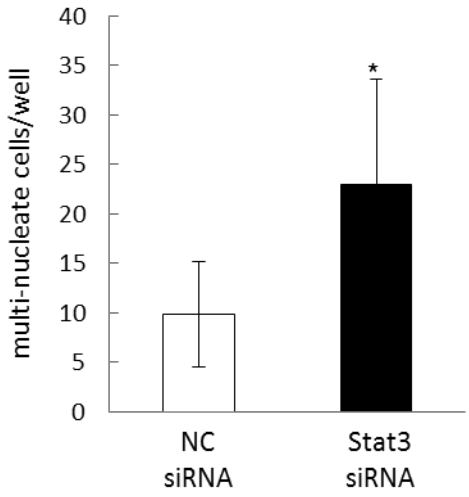

Figure 35: TRAP-stained RAW 264.7 cells stimulated with RANKL. A significant increase in multi-nucleated osteoclasts was observed when Stat3 was knocked down.

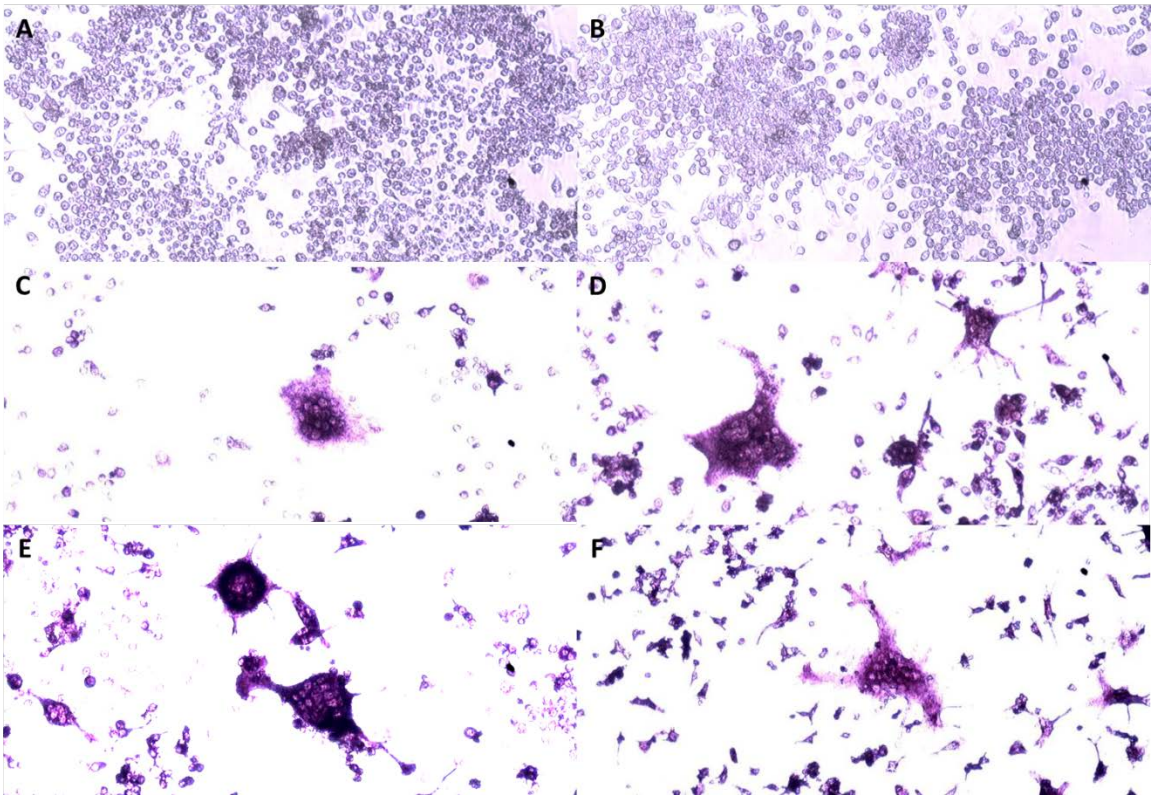

Figure 36: TRAP-stained RAW 264.7 cells. From left to right, top to bottom: non-specific siRNA without RANKL (A), Stat3 siRNA without RANKL (B), non-specific siRNA with RANKL (C,E), and Stat3 siRNA with RANKL (D,F).